Physica D 239 (2010) 1120–1134

Contents lists available at ScienceDirect

Physica D

journal homepage: www.elsevier.com/locate/physd

Comparisons between sine-Gordon and perturbed nonlinear Schrödinger equations for modeling light bullets beyond critical collapse

Weizhu Bao [a,*], Xuanchun Dong [a], Jack Xin [b]

[a] Department of Mathematics and Center for Computational Science and Engineering, National University of Singapore, Singapore 117543, Singapore
[b] Department of Mathematics, University of California at Irvine, Irvine, CA 92697, USA

ARTICLE INFO

Article history:
Received 18 April 2009
Received in revised form
2 March 2010
Accepted 8 March 2010
Available online 17 March 2010
Communicated by J. Garnier

Keywords:
Light bullets
Sine-Gordon equation
Perturbed NLS
Efficient numerical methods
Error bounds
Approximation beyond critical collapse

ABSTRACT

The sine-Gordon (SG) equation and perturbed nonlinear Schrödinger (NLS) equations are studied numerically for modeling the propagation of two space dimensional (2D) localized pulses (the so-called *light bullets*) in nonlinear dispersive optical media. We begin with the (2 + 1) SG equation obtained as an asymptotic reduction in the two level dissipationless Maxwell–Bloch system, followed by the review on the perturbed NLS equation in 2D for SG pulse envelopes, which is globally well posed and has all the relevant higher order terms to regularize the collapse of standard critical (cubic focusing) NLS. The perturbed NLS is approximated by truncating the nonlinearity into finite higher order terms undergoing focusing–defocusing cycles. Efficient semi-implicit sine pseudospectral discretizations for SG and perturbed NLS are proposed with rigorous error estimates. Numerical comparison results between light bullet solutions of SG and perturbed NLS as well as critical NLS are reported, which validate that the solution of the perturbed NLS as well as its finite-term truncations are in qualitative and quantitative agreement with the solution of SG for the light bullets propagation even after the critical collapse of cubic focusing NLS. In contrast, standard critical NLS is in qualitative agreement with SG only before its collapse. As a benefit of such observations, pulse propagations are studied via solving the perturbed NLS truncated by reasonably many nonlinear terms, which is a much cheaper task than solving SG equation directly.

1. Introduction

The propagation and interaction of spatially localized pulses (the so-called *light bullets*) with particle features in several space dimensions are of both physical and mathematical interests [1,2]. Such light bullets have been observed in the numerical simulations of the full Maxwell system with instantaneous Kerr ($\chi^{(3)}$ or cubic) nonlinearity in two space dimensions (2D) [3]. They are short femtosecond pulses that propagate without essentially changing shapes over a long distance and have only a few EM (electromagnetic) oscillations under their envelopes [3–7]. They have been found useful as information carriers in communication [5,8], as energy sources, switches and logic gates in optical devices [9].

In one space dimension (1D), the Maxwell system modeling light propagation in nonlinear media admits constant-speed traveling waves as exact solutions, also known as the *light bubbles* (unipolar pulses or solitons), [10–13]. The complete integrability of a Maxwell–Bloch system is shown in [14]. In several space dimensions, constant-speed traveling waves (mono-scale solutions) are harder to come by. Instead, space–time oscillating (multiple-scale) solutions are more robust [6]. The so-called light bullets are of multiple-scale structures with distinct phase/group velocities and amplitude dynamics. Even though direct numerical simulations of the full Maxwell system are motivating [3], asymptotic approximation is necessary for analysis in several space dimensions [6]. The approximation of 1D Maxwell system has been extensively studied. Long pulses are well approximated via envelope approximation by the cubic focusing nonlinear Schrödinger (NLS) for $\chi^{(3)}$ medium [8]. A comparison between Maxwell solutions and those of an extended NLS [4,5,15] also showed that the cubic NLS approximation works reasonably well on short stable 1D pulses. Mathematical analysis on the validity of NLS approximation of pulses and counter-propagating pulses of 1D sine-Gordon equation has been carried out [16,17]. However, in 2D, the envelope approximation with the cubic focusing NLS breaks down [18], because critical collapse of the cubic focusing NLS occurs in finite time (see [19–24] and the references therein). On the other hand, due to the intrinsic physical mechanism or material response, Maxwell system itself typically behaves fine beyond the cubic NLS collapse time. One example is the semi-classical two level dissipationless Maxwell–Bloch system where

* Corresponding author. Tel.: +65 6516 2765; fax: +65 6774 6756.
E-mail addresses: bao@math.nus.edu.sg (W. Bao), dong.xuanchun@nus.edu.sg (X. Dong), jxin@math.uci.edu (J. Xin).
URLs: http://www.math.nus.edu.sg/~bao/ (W. Bao), http://math.uci.edu/~jxin/ (J. Xin).

0167-2789/$ – see front matter © 2010 Elsevier B.V. All rights reserved.
doi:10.1016/j.physd.2010.03.002

smooth solutions persist forever [25]. It is thus a very interesting question how to modify the cubic NLS approximation to capture the correct physics for modeling the propagation and interaction of light signals in 2D Maxwell type systems.

Recently, by examining a distinguished asymptotic limit of the two level dissipationless Maxwell–Bloch system in the transverse electric regime, Xin [6] found that the well-known (2 + 1) sine-Gordon (SG) equation

$$\partial_{tt}u - c^2\nabla^2 u + \sin(u) = 0, \quad t > 0, \tag{1.1}$$

with initial conditions

$$u(\mathbf{x}, 0) = u^{(0)}(\mathbf{x}), \qquad \partial_t u(\mathbf{x}, 0) = u^{(1)}(\mathbf{x}), \quad \mathbf{x} = (x, y) \in \mathbb{R}^2, \tag{1.2}$$

where $u := u(\mathbf{x}, t)$ is a real-valued function and c is a given constant, has its own light bullets solutions. It is well known that the energy

$$E^{\mathrm{SG}}(t) := \int_{\mathbb{R}^2} \left[(\partial_t u)^2 + c^2|\nabla u|^2 + 2G(u)\right] \mathrm{d}\mathbf{x}, \quad t \geq 0, \tag{1.3}$$

with

$$G(u) = \int_0^u \sin(s)\mathrm{d}s = 1 - \cos(u), \tag{1.4}$$

is conserved in the above SG equation. Direct numerical simulations of the SG in 2D were performed [7,6], which are much simpler tasks than simulating the full Maxwell. Moving pulse solutions being able to keep the overall profile over a long time were observed, just like those in Maxwell system [3–5,7,6]. See also [26,27] for related breather-type solutions of SG in 2D based on a modulation analysis in the Lagrangian formulation. In [6], a new and complete perturbed NLS equation was derived by removing all resonance terms (*complete NLS approximation*) in carrying out the envelope expansion of SG. The new equation is second order in space–time and contains a nonparaxiality term, a mixed derivative term, and a novel nonlinear term which is saturating for large amplitude. The equation is globally well posed and does not have finite-time collapse.

The main purpose of this paper is to carry out comprehensive and accurate numerical comparisons between the solution of the SG equation and the solutions of the complete perturbed NLS and its finite-term approximation in nonlinearity, as well as the standard critical NLS. The computation challenge involved in SG simulation is that the disparate time scales between SG and perturbed NLS equations require a long-time simulation of SG equation in a large 2D domain, which need to be extended if the interested time point turns out to be further away due to the propagating property of SG light bullet solutions. On the other hand, for the perturbed NLS simulation the challenge is that high spatial resolution is required to capture the focusing–defocusing mechanism which prevents the critical NLS collapse. Here, semi-implicit sine pseudospectral discretizations are proposed, which can be explicitly solved in phase and are of spectral accuracy in space. Our results provide a numerical justification of the perturbed NLS as a valid approximation to SG in 2D, especially beyond the collapse time of cubic focusing NLS.

The rest of this paper is organized as follows. In Section 2, we review the derivation of the complete perturbed NLS from SG and approximate it by truncating the nonlinearity into finite higher order terms undergoing focusing–defocusing cycles. In Section 3, efficient semi-implicit sine pseudospectral discretizations for the SG and perturbed NLS are discussed. In Section 4, numerical results are reported on (1) the comparison between the solutions of SG and perturbed NLS with finite-time collapse present in the critical cubic NLS, (2) the study on the finite-term nonlinearity approximation and (3) the application to long-time propagation of pulses. Finally, concluding remarks are drawn in Section 5. Throughout the paper, we use the standard notations of Sobolev spaces with their corresponding norms. The notation $p \lesssim q$ means that there exists a constant $C > 0$, independent of mesh sizes and time steps, such that $|p| \leq Cq$.

2. Perturbed NLS and its approximations

As derived in [6], we look for a modulated planar pulse solution of SG (1.1) in the form:

$$u(\mathbf{x}, t) = \varepsilon A(\varepsilon(x - \nu t), \varepsilon y, \varepsilon^2 t)\mathrm{e}^{\mathrm{i}(kx-\omega(k)t)} + \text{c.c.} + \varepsilon^3 u_2, \quad \mathbf{x} = (x, y) \in \mathbb{R}^2, \quad t \geq 0, \tag{2.1}$$

where $0 < \varepsilon \ll 1$, $\omega = \omega(k) = \sqrt{1 + c^2k^2}$, $\nu = \omega'(k) = c^2k/\omega$, the group velocity, and c.c. refers to the complex conjugate of the previous term. Plugging (2.1) into (1.1), setting $X = \varepsilon(x - \nu t)$, $Y = \varepsilon y$ and $T = \varepsilon^2 t$, calculating derivatives, expressing the sine function in series and removing all the resonance terms, one obtains the following complete perturbed NLS (see details in [6]):

$$-2\mathrm{i}\omega\partial_T A + \varepsilon^2\partial_{TT}A = \frac{c^2}{\omega^2}\partial_{XX}A + c^2\partial_{YY}A + 2\varepsilon\nu\partial_{XT}A + |A|^2 A\sum_{l=0}^{\infty}\frac{(-1)^l(\varepsilon|A|)^{2l}}{(l+1)!(l+2)!}, \quad T > 0, \tag{2.2}$$

where $A := A(\mathbf{X}, T)$, $\mathbf{X} = (X, Y) \in \mathbb{R}^2$, is a complex-valued function.

Introducing the scaling variables $\widetilde{X} = (\omega/c)X$, $\widetilde{Y} = Y/c$ and $\widetilde{T} = T/(2\omega)$, substituting them into (2.2) and then removing all $\widetilde{\ }$, one gets a standard perturbed NLS,

$$\mathrm{i}\partial_T A - \frac{\varepsilon^2}{4\omega^2}\partial_{TT}A = -\nabla^2 A - \frac{\varepsilon c k}{\omega}\partial_{XT}A + f_\varepsilon\left(|A|^2\right)A, \quad T > 0, \tag{2.3}$$

with initial conditions,

$$A(\mathbf{X}, 0) = A^{(0)}(\mathbf{X}), \qquad \partial_T A(\mathbf{X}, 0) = A^{(1)}(\mathbf{X}), \quad \mathbf{X} \in \mathbb{R}^2, \tag{2.4}$$

where,

$$\rho = |A|^2, \qquad f_\varepsilon(\rho) = \sum_{l=0}^{\infty}\frac{(-1)^{l+1}\varepsilon^{2l}\rho^{l+1}}{(l+1)!(l+2)!}. \tag{2.5}$$

In fact, the Eq. (2.3) can be viewed as a perturbed cubic NLS with both a saturating nonlinearity (series) term and nonparaxial terms (the A_{TT} and A_{XT} terms). As proven in [6], it conserves the *energy*, i.e.,

$$E^{\mathrm{PNLS}}(T) := \int_{\mathbb{R}^2}\left[\frac{\varepsilon^2}{4\omega^2}|A_T|^2 + |\nabla A|^2 + F_\varepsilon\left(|A|^2\right)\right]\mathrm{d}\mathbf{X} \equiv E^{\mathrm{PNLS}}(0), \quad T \geq 0, \tag{2.6}$$

with

$$F_\varepsilon(\rho) = \int_0^\rho f_\varepsilon(s)\mathrm{d}s = \sum_{l=0}^{\infty}\frac{(-1)^{l+1}\varepsilon^{2l}\rho^{l+2}}{(l+1)!(l+2)!(l+2)}, \tag{2.7}$$

and has the *mass* balance identity

$$\frac{\mathrm{d}}{\mathrm{d}T}\left(\int_{\mathbb{R}^2}|A|^2\mathrm{d}\mathbf{X} - \frac{\varepsilon^2}{2\omega^2}\mathrm{Im}\int_{\mathbb{R}^2}A_T\bar{A}\mathrm{d}\mathbf{X}\right) = \frac{2\varepsilon\nu}{c}\mathrm{Im}\int A_X\overline{A_T}\mathrm{d}\mathbf{X}, \tag{2.8}$$

where $\bar{f}$ denotes the conjugate of f. In addition, the perturbed NLS (2.3) is globally well posed and does not have finite-time collapse [6], i.e., for any given initial data $A^{(0)}(\mathbf{X}) \in H^2(\mathbb{R}^2)$ and

$A^{(1)}(\mathbf{X}) \in H^1(\mathbb{R}^2)$, the initial value problem of (2.3) with initial conditions (2.4) has a unique global solution $A \in C([0,\infty]; H^2(\mathbb{R}^2))$, $A_T \in C([0,\infty]; H^1(\mathbb{R}^2))$, and $A_{TT} \in C([0,\infty]; L^2(\mathbb{R}^2))$.

In practice, the infinite series of the nonlinearity in (2.3) is usually truncated to finite terms with focusing–defocusing cycles. Denote

$$f_\varepsilon^N(\rho) = \sum_{l=0}^{N} \frac{\varepsilon^{4l}\rho^{2l+1}}{(2l+1)!(2l+2)!}\left[-1+\frac{\varepsilon^2\rho}{(2l+2)(2l+3)}\right], \quad (2.9)$$

then the perturbed NLS (2.3) can be approximated by the following truncated NLS:

$$\mathrm{i}\partial_T A - \frac{\varepsilon^2}{4\omega^2}\partial_{TT}A = -\nabla^2 A - \frac{\varepsilon c k}{\omega}\partial_{XT}A + f_\varepsilon^N\left(|A|^2\right)A, \quad T>0. \quad (2.10)$$

Similar as the proof in [6] for perturbed NLS (2.3), one can show that the truncated NLS (2.10) with the initial conditions (2.4) also conserves the *energy*, i.e.,

$$E_N^{\mathrm{PNLS}}(T) := \int_{\mathbb{R}^2}\left[\frac{\varepsilon^2}{4\omega^2}|A_T|^2 + |\nabla A|^2 + F_\varepsilon^N\left(|A|^2\right)\right]\mathrm{d}\mathbf{X} \equiv E_N^{\mathrm{PNLS}}(0), \quad T\geq 0, \quad (2.11)$$

with

$$F_\varepsilon^N(\rho) = \int_0^\rho f_\varepsilon^N(s)\mathrm{d}s = \sum_{l=0}^{N}\frac{\varepsilon^{4l}\rho^{2l+2}}{(2l+1)!(2l+2)!(2l+2)}\left[-1+\frac{\varepsilon^2\rho}{(2l+3)^2}\right], \quad (2.12)$$

and has the *mass* balance identity (2.8).

When $\varepsilon = 0$, the perturbed NLS (2.3) and its approximation (2.10) collapse to the well-known cubic (critical) focusing NLS:

$$\mathrm{i}\partial_T A = -\nabla^2 A - \frac{1}{2}|A|^2 A, \quad T>0, \quad (2.13)$$

with initial condition,

$$A(\mathbf{X},0) = A^{(0)}(\mathbf{X}), \quad \mathbf{X}\in\mathbb{R}^2. \quad (2.14)$$

It is well known that this cubic NLS conserves the energy, i.e.,

$$E^{\mathrm{CNLS}}(T) := \int_{\mathbb{R}^2}\left[|\nabla A|^2 - \frac{1}{4}|A|^4\right]\mathrm{d}\mathbf{X} \equiv \int_{\mathbb{R}^2}\left[\left|\nabla A^{(0)}\right|^2 - \frac{1}{4}|A^{(0)}|^4\right]\mathrm{d}\mathbf{X}, \quad (2.15)$$

and when the initial energy $E^{\mathrm{CNLS}}(0) < 0$, finite-time collapse occurs in this focusing cubic (critical) NLS [23,24,19], which motivates different choices of initial data in (2.4) and (2.14) for our numerical experiments.

We remark here that as mentioned in the introduction, noting (2.1) the disparate time scales for the perturbed NLS equations (2.10) and the SG equation (1.1) are $T = O(1)$ and $t = O(\varepsilon^{-2})$, respectively, which immediately implies that it requires a much longer time simulation for the SG equation (1.1) if the time regime beyond the collapse time of the critical NLS (2.13) is of interest, when ε is small.

3. Numerical methods for SG and perturbed NLS

Various finite difference discretizations for the SG [28–31] and NLS equation [32,33] were proposed in the literatures, which are only of polynomial order accuracy in space. Here we will present efficient semi-implicit sine pseudospectral approximations [34,35] for the SG (1.1) and perturbed NLS (2.10), which are of spectral accuracy in space and efficient in computation.

Since we are interested in the finite-time propagation of the light bullets, noting the inherent far-field vanishing property of the light bullets solutions of SG and NLS equations, in practice, we always truncate the whole space problems on a bounded computational domain Ω, e.g. $\Omega = [a,b]\times[c,d]$, with homogeneous Dirichlet boundary conditions. Let $\Delta t > 0$ be the time step and denote time steps as $t_n = n\Delta t$, $n = 0, 1, \ldots$; choose spatial mesh sizes $\Delta x = \frac{b-a}{J}$ and $\Delta y = \frac{d-c}{K}$ with J, K being two positive even integers, and denote the grid points be

$$x_j := a + j\Delta x, \quad j = 0,1,\ldots,J;$$
$$y_k := c + k\Delta y, \quad k = 0,1,\ldots,K.$$

Let

$$Y_{JK} = \mathrm{span}\{\phi_{lm}(\mathbf{x}),\ l = 1,2,\ldots,J-1,\ m = 1,2,\ldots,K-1\},$$

where

$$\phi_{lm}(\mathbf{x}) := \sin(\mu_l(x-a))\sin(\lambda_m(y-c)), \quad \mathbf{x} = (x,y)\in\mathbb{R}^2,$$
$$\mu_l = \pi l/(b-a), \quad \lambda_m = \pi m/(d-c), \quad l = 1,2,\ldots,J-1,\ m = 1,2,\ldots,K-1.$$

For a function $\xi(\mathbf{x}) \in L_0^2(\Omega) = \{v(\mathbf{x}) | v\in L^2(\Omega), v|_{\partial\Omega} = 0\}$ and a matrix $\varphi := \{\varphi_{jk}\}_{j,k=0}^{J,K} \in \mathbb{C}_0^{(J+1)(K+1)} = \{w\in\mathbb{C}^{(J+1)(K+1)} | w_{0k} = w_{Jk} = w_{j0} = w_{jK} = 0,\ j = 0,1,\ldots,J,\ k = 0,1,\ldots,K\}$, denote $P_{JK} : L_0^2(\Omega) \to Y_{JK}$ and $I_{JK} : \mathbb{C}_0^{(J+1)(K+1)} \to Y_{JK}$ be the standard projection and trigonometric interpolation operators [36,37], respectively, i.e.,

$$(P_{JK}\xi)(\mathbf{x}) = \sum_{l=1}^{J-1}\sum_{m=1}^{K-1}\widehat{\xi}_{lm}\phi_{lm}(\mathbf{x}),$$

$$(I_{JK}\varphi)(\mathbf{x}) = \sum_{l=1}^{J-1}\sum_{m=1}^{K-1}\widetilde{\varphi}_{lm}\phi_{lm}(\mathbf{x}), \quad \mathbf{x}\in\Omega, \quad (3.1)$$

where

$$\widehat{\xi}_{lm} = \frac{4}{(b-a)(d-c)}\int_\Omega \xi(\mathbf{x})\phi_{lm}(\mathbf{x})\mathrm{d}\mathbf{x},$$

$$\widetilde{\varphi}_{lm} = \frac{4}{JK}\sum_{j=1}^{J-1}\sum_{k=1}^{K-1}\varphi_{jk}\phi_{lm}(x_j,y_k), \quad (3.2)$$

$$\widetilde{\xi}_{lm} = \frac{4}{JK}\sum_{j=1}^{J-1}\sum_{k=1}^{K-1}\xi(x_j,y_k)\phi_{lm}(x_j,y_k), \quad l = 1,\ldots,J-1,\ m = 1,\ldots,K-1. \quad (3.3)$$

Semi-implicit sine pseudospectral method for the SG equation. Let $u_{JK}^n(\mathbf{x})$ be the approximation of $u(\mathbf{x},t_n)$ ($\mathbf{x}\in\Omega$), and respectively, u_{jk}^n be the approximation of $u(x_j,y_k,t_n)$ ($j = 0,1,\ldots,J, k = 0,1,\ldots,K$) and denote u^n be the matrix with components u_{jk}^n at time $t = t_n$. Choose $u_{JK}^0(\mathbf{x}) = P_{JK}(u^{(0)})$ for $\mathbf{x}\in\Omega$, by applying the sine spectral method for spatial derivatives and second order implicit and explicit schemes for linear and nonlinear terms, respectively, in time discretization for the SG equation (1.1), we get the semi-implicit sine spectral discretization as:

Find $u_{JK}^{n+1}(\mathbf{x}) \in Y_{JK}$, i.e.,

$$u_{JK}^{n+1}(\mathbf{x}) = \sum_{l=1}^{J-1}\sum_{m=1}^{K-1}\widehat{(u_{JK}^{n+1})}_{lm}\phi_{lm}(\mathbf{x}), \quad \mathbf{x}\in\Omega,\ n\geq 0, \quad (3.4)$$

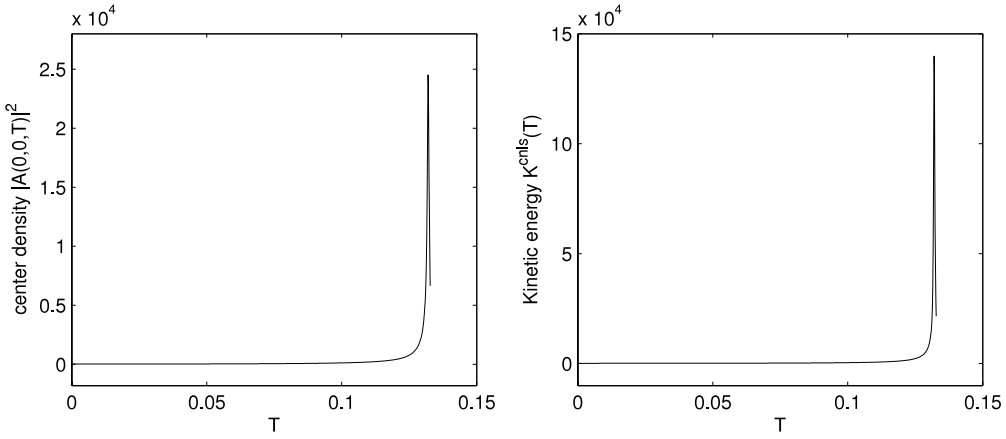

Fig. 1. Evolution of center density $|A(0,0,T)|^2$ and kinetic energy $K^{\mathrm{cnls}}(T)$ for cubic NLS with initial data chosen as (4.5) and $a_0 = 5.2$, numerically implying blow-up happens at $T^* \approx 0.1310$.

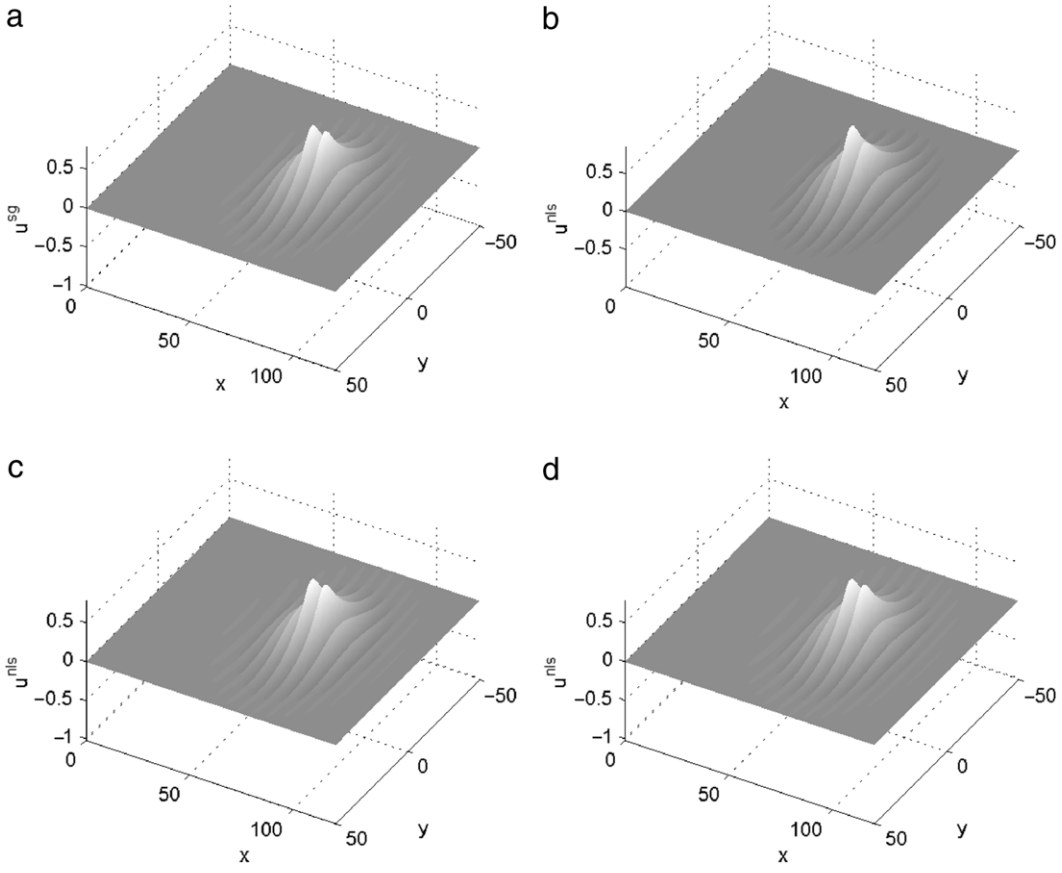

Fig. 2. Surface plots of the numerical solutions of u^{sg} and u^{nls} at $t = 115.2$ in the SG time scale which corresponds to $T = 0.095 < T^*$ (well before collapse of cubic NLS) in the NLS time scale for $\varepsilon = 0.05$ and $k = 1$. (a) SG solution; (b) cubic NLS solution; (c) perturbed NLS solution with $N = 0$; and (d) perturbed NLS solution with $N = 1$.

such that for $\mathbf{x} \in \Omega$ and $n \geq 1$,

$$\frac{u_{JK}^{n+1} - 2u_{JK}^{n} + u_{JK}^{n-1}}{(\Delta t)^2} - \frac{c^2}{2}\left(\nabla^2 u_{JK}^{n+1} + \nabla^2 u_{JK}^{n-1}\right) + P_{JK}\left(\sin(u_{JK}^{n})\right) = 0, \tag{3.5}$$

and the initial data in (1.2) is discretized as

$$\frac{u_{JK}^{1} - u_{JK}^{0}}{\Delta t} = P_{JK}(u^{(1)}) + \frac{\Delta t}{2}\left[c^2\nabla^2 u_{JK}^{0} - P_{JK}\left(\sin(u^{(0)})\right)\right]. \tag{3.6}$$

Plugging (3.4) into (3.6) and (3.5) and noticing the orthogonality of sine functions, for $l = 1, 2, \ldots, J-1$ and $m = 1, 2, \ldots, K-1$, we get

$$\widehat{\left(u_{JK}^{n+1}\right)}_{lm} = \begin{cases} \left[1 - \frac{c^2}{2}(\Delta t)^2\left(\mu_l^2 + \lambda_m^2\right)\right]\widehat{\left(u^{(0)}\right)}_{lm} + \Delta t\,\widehat{\left(u^{(1)}\right)}_{lm} \\ \quad - \frac{(\Delta t)^2}{2}\widehat{\left(\sin(u^{(0)})\right)}_{lm}, \quad n = 0, \\ \frac{2}{2 + c^2(\Delta t)^2(\mu_l^2 + \lambda_m^2)}\left[2\widehat{\left(u_{JK}^{n}\right)}_{lm}\right. \\ \quad \left. - (\Delta t)^2\widehat{\left(\sin(u_{JK}^{n})\right)}_{lm}\right] - \widehat{\left(u_{JK}^{n-1}\right)}_{lm}, \quad n \geq 1. \end{cases}$$

The above discretization scheme (3.5)–(3.6) is spectral order accurate in space and second-order accurate in time; in fact, as proven in the Appendix A, we have the following error estimate,

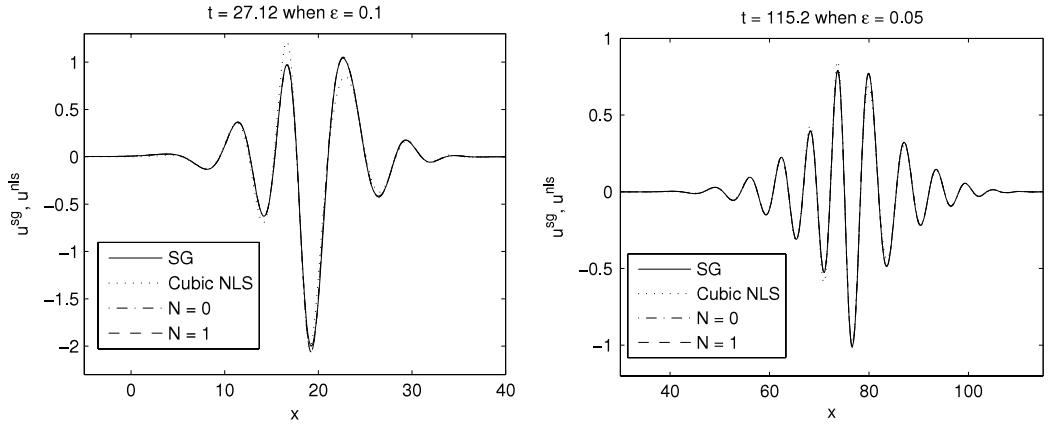

Fig. 3. Slice plots of the numerical solutions of u^{sg} and u^{nls} along x-axis with $y = 0$ for $k = 1$. Left column: for $\varepsilon = 0.1$ at $t = 27.12$; right column: for $\varepsilon = 0.05$ at $t = 115.2$.

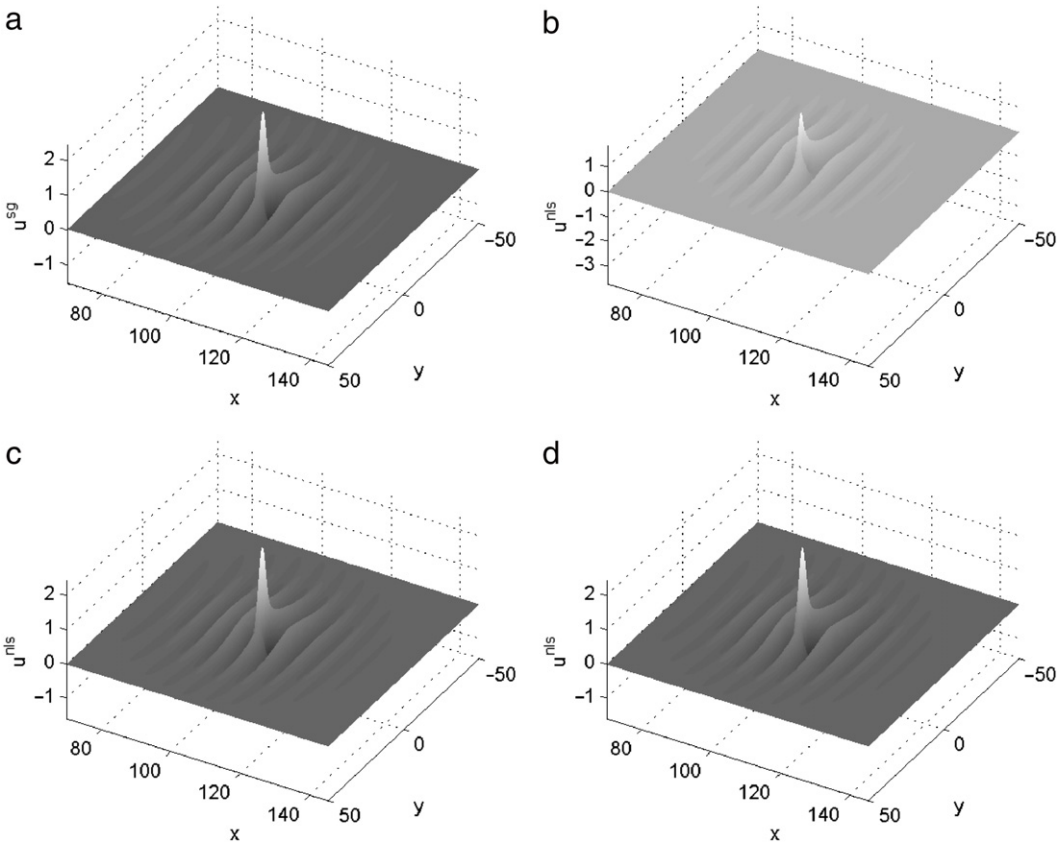

Fig. 4. Surface plots of the numerical solutions of u^{sg} and u^{nls} at $t = 148.16$ in the SG time scale which corresponds to $T = 0.1310 \approx T^*$ (near collapse of cubic NLS) in the NLS time scale for $\varepsilon = 0.05$ and $k = 1$. (a) SG solution; (b) cubic NLS solution; (c) perturbed NLS solution with $N = 0$; and (d) perturbed NLS solution with $N = 1$.

Theorem 3.1. *Let $t^* > 0$ be a fixed time and suppose the exact solution $u(\mathbf{x}, t)$ of the problem (1.1)–(1.2) satisfying $u(\mathbf{x}, t) \in C^4\left([0, t^*]; L^2(\Omega)\right) \cap C^3\left([0, t^*]; H^1(\Omega)\right) \cap C^2\left([0, t^*]; H^2(\Omega)\right) \cap C\left([0, t^*]; H_0^1(\Omega) \cap H^m(\Omega)\right)$ for some $m \geq 2$. Let $u_{jk}^n(\mathbf{x})$ be the approximations obtained from (3.5)–(3.6), then there exist two positive constants k_0 and h_0, such that for any $0 < \Delta t \leq k_0$ and $0 < h := \max\{\Delta x, \Delta y\} \leq h_0$, we have*

$$\left\|\mathrm{e}^n(\mathbf{x})\right\|_{L^2(\Omega)} \lesssim (\Delta t)^2 + h^m,$$

$$\left\|\mathrm{e}^n(\mathbf{x})\right\|_{H^1(\Omega)} \lesssim (\Delta t)^2 + h^{m-1}, \quad 0 \leq n \leq \frac{t^*}{\Delta t}, \tag{3.7}$$

where $\mathrm{e}^n(\mathbf{x}) = u(\mathbf{x}, t_n) - u_{jK}^n(\mathbf{x})$.

In fact, the above procedure is not suitable in practice due to the difficulty of computing the integrals in (3.5), (3.6) and (3.2). However, it can be used to serve as a prototype for designing the pseudospectral method. We now present an efficient implementation via approximating the integrals in (3.5), (3.6) and (3.2) by a quadrature rule on the grids $\{(x_j, y_k),\ j = 0, 1, \ldots, J,\ k = 0, 1, \ldots, K\}$. Choose $u_{jk}^0 = u^{(0)}(x_j, y_k)$ $(j = 0, 1, \ldots, J, k = 0, 1, \ldots, M)$, for $n = 0, 1, \ldots$, the semi-implicit sine pseudospectral discretization for the problem (1.1)–(1.2) reads

$$u_{jk}^{n+1} = \sum_{l=1}^{J-1} \sum_{m=1}^{K-1} \widetilde{\left(u^{n+1}\right)}_{lm} \phi_{lm}(x_j, y_k),$$
$$j = 0, 1, \ldots, J,\ k = 0, 1, \ldots, K, \tag{3.8}$$

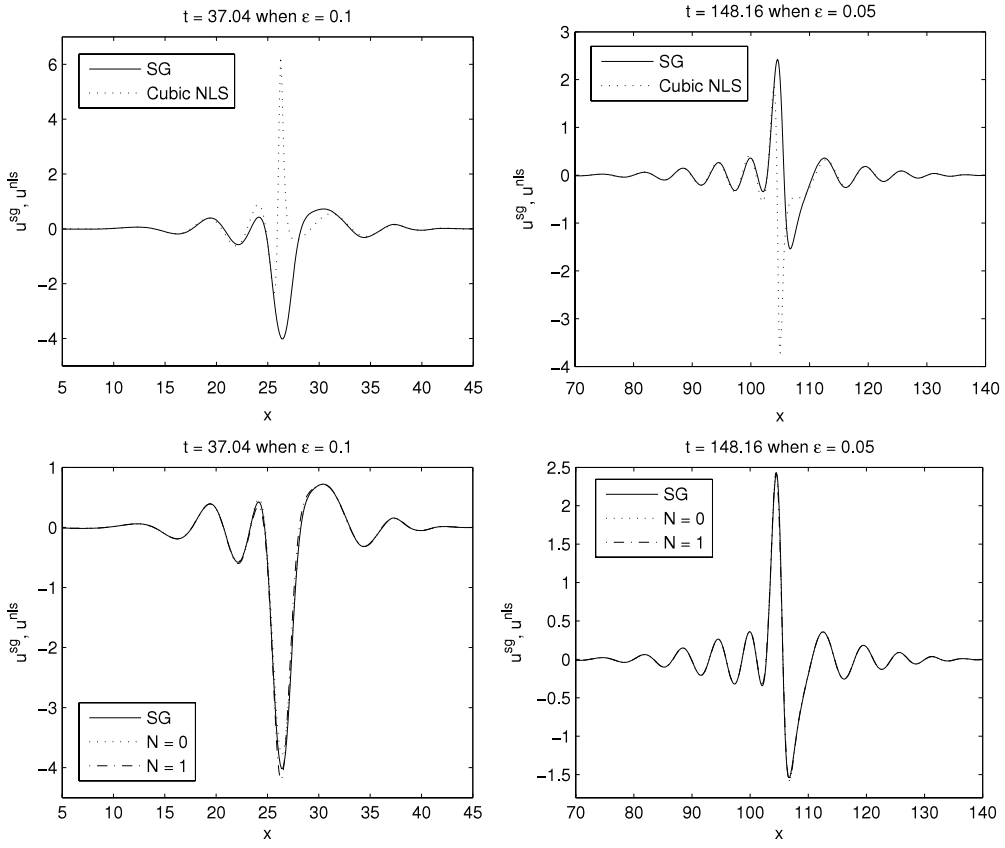

Fig. 5. Slice plots of the numerical solutions of $u^{\rm sg}$ and $u^{\rm nls}$ along x-axis with $y = 0$ for $k = 1$. Top row: comparison of SG and cubic NLS; Bottom row: comparison of SG and perturbed NLS with different N.

where

$$\widetilde{\left(u^{n+1}\right)}_{lm} = \begin{cases} \left[1 - \dfrac{c^2}{2}(\Delta t)^2\left(\mu_l^2 + \lambda_m^2\right)\right]\widetilde{\left(u^{(0)}\right)}_{lm} + \Delta t\widetilde{\left(u^{(1)}\right)}_{lm} \\ \quad - \dfrac{(\Delta t)^2}{2}\widetilde{\left(\sin(u^{(0)})\right)}_{lm}, \quad n = 0; \\ \dfrac{2}{2 + c^2(\Delta t)^2(\mu_l^2 + \lambda_m^2)}\left[2\widetilde{(u^n)}_{lm}\right. \\ \quad \left. - (\Delta t)^2\widetilde{(\sin(u^n))}_{lm}\right] - \widetilde{(u^{n-1})}_{lm}, \quad n \geq 1. \end{cases}$$

Again, this scheme is spectral order accurate in space and second-order accurate in time. It is explicitly solvable in phase space, the memory cost is $O(JK)$ and computational cost per time step is $O(JK \ln(JK))$ via fast discrete sine transform (DST), thus it is very efficient in computation.

Semi-implicit sine pseudospectral method for the perturbed NLS equations. Let $\Delta T > 0$ be the time step and denote time steps as $T_n = n\Delta T$, $n = 0, 1, \ldots$; and we choose spatial mesh sizes ΔX and ΔY and grid points X_j $(j = 0, 1, \ldots, J)$ and Y_k $(k = 0, 1, \ldots, K)$ in a similar manner as Δx and Δy as well as x_j and y_k. Let $A_{JK}^n(\mathbf{X})$ be the approximation of $A(\mathbf{X}, T_n)$ $(\mathbf{X} \in \Omega)$, and respectively, A_{jk}^n be the approximation of $A(X_j, Y_k, T_n)$ $(j = 0, 1, \ldots, J,\ k = 0, 1, \ldots, K)$ and denote A^n be the matrix with components A_{jk}^n at time $T = T_n$. Choose $A_{JK}^0(\mathbf{X}) = P_{JK}(A^{(0)})$ for $\mathbf{X} \in \Omega$, by applying the sine spectral method for spatial derivatives and second order implicit and explicit schemes for linear and nonlinear terms, respectively, in time discretization for the perturbed NLS equation (2.10), we get the semi-implicit sine spectral discretization as:

Find $A_{JK}^{n+1}(\mathbf{X}) \in Y_{JK}$, i.e.,

$$A_{JK}^{n+1}(\mathbf{X}) = \sum_{l=1}^{J-1}\sum_{m=1}^{K-1}\widehat{\left(A_{JK}^{n+1}\right)}_{lm}\phi_{lm}(\mathbf{X}), \quad \mathbf{X} \in \Omega,\ n \geq 0, \tag{3.9}$$

such that for $\mathbf{X} \in \Omega$ and $n \geq 1$

$$\begin{aligned} &\mathrm{i}\frac{A_{JK}^{n+1} - A_{JK}^{n-1}}{2\Delta T} \\ &\quad = \frac{\varepsilon^2}{4\omega^2}\frac{A_{JK}^{n+1} - 2A_{JK}^n + A_{JK}^{n-1}}{(\Delta T)^2} - \frac{\varepsilon ck}{2\omega\Delta T}\left(\partial_X A_{JK}^{n+1} - \partial_X A_{JK}^{n-1}\right) \\ &\qquad - \frac{1}{2}\left(\nabla^2 A_{JK}^{n+1} + \nabla^2 A_{JK}^{n-1}\right) + P_{JK}\left(f_\varepsilon^N\left(|A_{JK}^n|^2\right)A_{JK}^n\right), \end{aligned} \tag{3.10}$$

and the initial data in (2.4) is discretized as

$$\begin{aligned} \frac{A_{JK}^1 - A_{JK}^0}{\Delta T} &= P_{JK}(A^{(1)}) + \frac{4\omega^2\Delta T}{2\varepsilon^2}\left[\mathrm{i}P_{JK}(A^{(1)}) + \nabla^2 A_{JK}^0\right. \\ &\quad \left. + \frac{\varepsilon ck}{\omega}\partial_X P_{JK}(A^{(1)}) - P_{JK}\left(f_\varepsilon^N(|A^{(0)}|^2)A^{(0)}\right)\right]. \end{aligned} \tag{3.11}$$

Plugging (3.9) into (3.10) and (3.11) and noticing the orthogonality of sine functions, for $l = 1, 2, \ldots, J-1$ and $m = 1, 2, \ldots, K-1$, we obtain

$$\widehat{\left(A_{JK}^{n+1}\right)}_{lm} = \begin{cases} \alpha_{lm}\widehat{\left(A^{(0)}\right)}_{lm} + \beta_{lm}\widehat{\left(A^{(1)}\right)}_{lm} \\ \quad - \dfrac{2\omega^2(\Delta T)^2}{\varepsilon^2}\widehat{\left(g^0\right)}_{lm}, \quad n = 0; \\ \dfrac{\mathrm{i} - \gamma_{lm}}{\mathrm{i} + \gamma_{lm}}\widehat{\left(A_{JK}^{n-1}\right)}_{lm} - \dfrac{\varepsilon^2}{\omega^2\Delta T\,(\mathrm{i} + \gamma_{lm})}\widehat{\left(A_{JK}^n\right)}_{lm} \\ \quad + \dfrac{2\Delta T}{\mathrm{i} + \gamma_{lm}}\widehat{\left(g^n\right)}_{lm}, \quad n \geq 1, \end{cases}$$

where

$$\alpha_{lm} = 1 - \frac{2\omega^2(\Delta T)^2}{\varepsilon^2}\left(\mu_l^2 + \lambda_m^2\right),$$

$$\beta_{lm} = \Delta T + \frac{\mathrm{i}2\omega^2(\Delta T)^2}{\varepsilon^2} + \frac{\mathrm{i}2\omega ck\mu_l(\Delta T)^2}{\varepsilon},$$

$$\gamma_{lm} = -\Delta T\left(\mu_l^2+\lambda_m^2\right) - \frac{\varepsilon^2}{2\omega^2\Delta T} + \frac{\mathrm{i}\varepsilon ck\mu_l}{\omega},$$
$$1\le l\le J-1,\ 1\le m\le K-1,$$

$$g^0(\mathbf{X}) = f_\varepsilon^N\left(|A^{(0)}(\mathbf{X})|^2\right)A^{(0)}(\mathbf{X}),$$

$$g^n(\mathbf{X}) = f_\varepsilon^N\left(|A_{JK}^n(\mathbf{X})|^2\right)A_{JK}^n(\mathbf{X}),\quad n\ge 1,\ \mathbf{X}\in\Omega.$$

Similarly, the above discretization scheme (3.10)–(3.11) is spectral order accurate in space and second-order accurate in time; in fact, as proven in the Appendix B, we have the following error estimate,

Theorem 3.2. *Let $\varepsilon = \varepsilon_0$ be a fixed constant in (2.10) and $T^* > 0$ be any fixed time, suppose the exact solution $A(\mathbf{X}, T)$ of the problem (2.10) with (2.4) satisfying $A(\mathbf{X}, T)\in C^4\left([0, T^*]; L^2(\Omega)\right)\cap C^3\left([0, T^*]; H^1(\Omega)\right)\cap C^2\left([0, T^*]; H^2(\Omega)\right)\cap C([0, T^*]; H_0^1(\Omega)\cap H^m(\Omega)\cap L^\infty(\Omega))$ for some $m\ge 2$. Let A_{JK}^n be the approximations obtained from (3.10) and (3.11) at time $T = T_n$, then there exist two positive constants k_0 and h_0, such that for any $0\le\Delta T\le k_0$ and $0 < h := \max\{\Delta X, \Delta Y\}\le h_0$, satisfying $\Delta T\le\kappa h_{\min} := \min\{\Delta X, \Delta Y\}$ and $h\le\kappa h_{\min}$ with a positive constant $\kappa > 0$, we have,*

$$\left\|\mathrm{e}^n(\mathbf{X})\right\|_{L^2(\Omega)}\lesssim(\Delta T)^2+h^m,$$

$$\left\|\mathrm{e}^n(\mathbf{X})\right\|_{H^1(\Omega)}\lesssim(\Delta T)^2+h^{m-1},\quad 0\le n\le\frac{T^*}{\Delta T},\tag{3.12}$$

where $\mathrm{e}^n(\mathbf{X}) = A(\mathbf{X}, T_n) - A_{JK}^n(\mathbf{X})$.

Again, the above procedure is not suitable in practice due to the difficulty of computing the integrals in (3.10), (3.11) and (3.2). Similarly, it can be used to serve as a prototype for designing the pseudospectral method. Choose $A_{jk}^0 = A^{(0)}(X_j, Y_k)$ ($j = 0, 1, \ldots, J$, $k = 0, 1, \ldots, M$), for $n = 0, 1, \ldots,$ the semi-implicit sine pseudospectral discretization for the problem (2.10) with (2.4) reads

$$A_{jk}^{n+1} = \sum_{l=1}^{J-1}\sum_{m=1}^{K-1}\widetilde{\left(A^{n+1}\right)}_{lm}\phi_{lm}(X_j, Y_k),$$
$$j = 0, 1, \ldots, J,\ k = 0, 1, \ldots, K,\tag{3.13}$$

where

$$\widetilde{\left(A^{n+1}\right)}_{lm} = \begin{cases}\alpha_{lm}\widetilde{\left(A^{(0)}\right)}_{lm} + \beta_{lm}\widetilde{\left(A^{(1)}\right)}_{lm}\\ \quad -\dfrac{2\omega^2(\Delta T)^2}{\varepsilon^2}\widetilde{\left(g^0\right)}_{lm}, & n = 0;\\ \dfrac{\mathrm{i}-\gamma_{lm}}{\mathrm{i}+\gamma_{lm}}\widetilde{\left(A^{n-1}\right)}_{lm} - \dfrac{\varepsilon^2}{\omega^2\Delta T\,(\mathrm{i}+\gamma_{lm})}\widetilde{\left(A^n\right)}_{lm}\\ \quad +\dfrac{2\Delta T}{\mathrm{i}+\gamma_{lm}}\widetilde{\left(g^n\right)}_{lm}, & n\ge 1;\end{cases}$$

where

$$g_{jk}^n = f_\varepsilon^N\left(|A_{jk}^n|^2\right)A_{jk}^n,\quad 0\le j\le J,\ 0\le k\le K,\ n\ge 0.$$

Again, this scheme is spectral order accurate in space and second-order accurate in time. It is explicitly solvable in phase space, the memory cost is $O(JK)$ and computational cost per time step is $O(JK\ln(JK))$ via DST, thus it is very efficient in computation.

4. Numerical experiments

In this section, we shall numerically study SG, perturbed NLS (2.10) with different N and cubic NLS (2.13) for modeling light bullets, concerning with comparisons among them, as well as looking at the propagating pulses via solving perturbed NLS (2.10) with N large enough. The studies mainly focus on the regime beyond critical collapse in cubic NLS. The SG and perturbed NLS equations are solved by the efficient methods proposed in the previous section, and the cubic NLS is discretized by the efficient and accurate time-splitting pseudospectral method [34,35]. In simulation, we take $c = 1$ in (1.1) and choose the initial data $A^{(0)}(\mathbf{X})$ in (2.4) and (2.14) such that it decays to zero sufficiently fast as $|\mathbf{X}|\to\infty$. In order to make the perturbed NLS (2.10) is consistent with the cubic NLS (2.13) at $T = 0$ when $\varepsilon\to 0$, the initial data $A^{(1)}(\mathbf{X})$ in (2.4) is chosen as

$$A^{(1)}(\mathbf{X}) = \mathrm{i}\left[\nabla^2A^{(0)}(\mathbf{X}) + \frac{1}{2}\left|A^{(0)}(\mathbf{X})\right|A^{(0)}(\mathbf{X})\right],\quad \mathbf{X}\in\mathbb{R}^2.\tag{4.1}$$

From the ansatz (2.1) with $t = 0$ and omitting all $O(\varepsilon^3)$ terms, the initial data in (1.2) for the SG equation can be chosen as

$$u^{(0)}(\mathbf{x}) = \varepsilon\left[\cos(kx)\left(A^{(0)}+\overline{A^{(0)}}\right)+\mathrm{i}\sin(kx)\left(A^{(0)}-\overline{A^{(0)}}\right)\right],$$
$$\mathbf{x}\in\mathbb{R}^2,\tag{4.2}$$

$$u^{(1)}(\mathbf{x}) = \varepsilon\omega\left[\mathrm{i}\cos(kx)\left(\overline{A^{(0)}}-A^{(0)}\right)+\sin(kx)\left(\overline{A^{(0)}}+A^{(0)}\right)\right]$$
$$-\varepsilon^2k\Big[\cos(kx)\partial_X\left(A^{(0)}+\overline{A^{(0)}}\right)$$
$$+\mathrm{i}\sin(kx)\partial_X\left(A^{(0)}-\overline{A^{(0)}}\right)\Big],\tag{4.3}$$

where

$$A^{(0)} = A^{(0)}(\mathbf{X}) = A^{(0)}(\varepsilon\omega x, \varepsilon y),\quad X = \varepsilon\omega x,\quad Y = \varepsilon y,\quad \mathbf{X}\in\mathbb{R}^2.$$

With the solution A_{jk}^n of the perturbed NLS (2.10) or the cubic NLS (2.13), we construct the envelope solution of NLS-type equations as

$$u^{\mathrm{nls}}(\mathbf{x}, t) = \varepsilon A\left(\frac{\omega\varepsilon(x-\nu t)}{c}, \frac{\varepsilon y}{c}, \frac{\varepsilon^2 t}{2\omega}\right)\mathrm{e}^{\mathrm{i}(kx-\omega t)}+\mathrm{c.c.},$$
$$\mathbf{x}\in\mathbb{R}^2,\ t\ge 0.\tag{4.4}$$

We always compute on a domain large enough such that the zeros boundary conditions do not introduce a significant aliasing error relative to the problem in whole space. Also, in all the results below, we observed that there is no substantial improvement in the numerical results by refining the mesh sizes and time steps.

4.1. Comparisons when finite-time collapse occurs in cubic NLS

We take the initial data in (2.4) and (2.14) as

$$A_0(\mathbf{X}) = \mathrm{i}a_0\ \mathrm{sech}\left(\frac{X^2+Y^2}{\sigma^2}\right),\quad \mathbf{X}\in\mathbb{R}^2,\tag{4.5}$$

with $a_0 = 5.2$ and $\sigma^2 = 0.8$ such that $E^{\mathrm{CNLS}}(0) < 0$ and thus finite-time collapse will appear in the cubic NLS Eq. (2.13). Again, plugging (4.5) into (4.2) and (4.3), we immediately get the initial conditions in this case for the SG equation (1.1) as

$$u^{(0)}(\mathbf{x}) = -2a_0\varepsilon\ \mathrm{sech}\left(\frac{\varepsilon^2(\omega^2x^2+y^2)}{\sigma^2}\right)\sin(kx),\quad \mathbf{x}\in\mathbb{R}^2,\tag{4.6}$$

$$u^{(1)}(\mathbf{x})$$
$$= -\omega u^{(0)}(\mathbf{x})\left[\cot(kx) - \frac{2\varepsilon^2kx}{\sigma^2}\tanh\left(\frac{\varepsilon^2(\omega^2x^2+y^2)}{\sigma^2}\right)\right],\tag{4.7}$$

with $\omega = \sqrt{1+k^2}$ and we take $k = 1$.

Here we report numerical results for $\varepsilon = 0.1$ and $\varepsilon = 0.05$, comparing the approximated light bullet solutions of SG and perturbed NLS as well as cubic NLS at three typical time regimes, i.e., before, near and after the collapse time $T = T^*\approx 0.1310$ of the cubic NLS. Here, T^* is numerically found by looking at the evolution of either center density $|A(0, 0, T)|^2$ or kinetic energy $K^{\mathrm{cnls}} := \int_\Omega\frac{1}{2}\|\nabla A(\mathbf{X}, T)\|^2\,\mathrm{d}\mathbf{X}$; see Fig. 1.

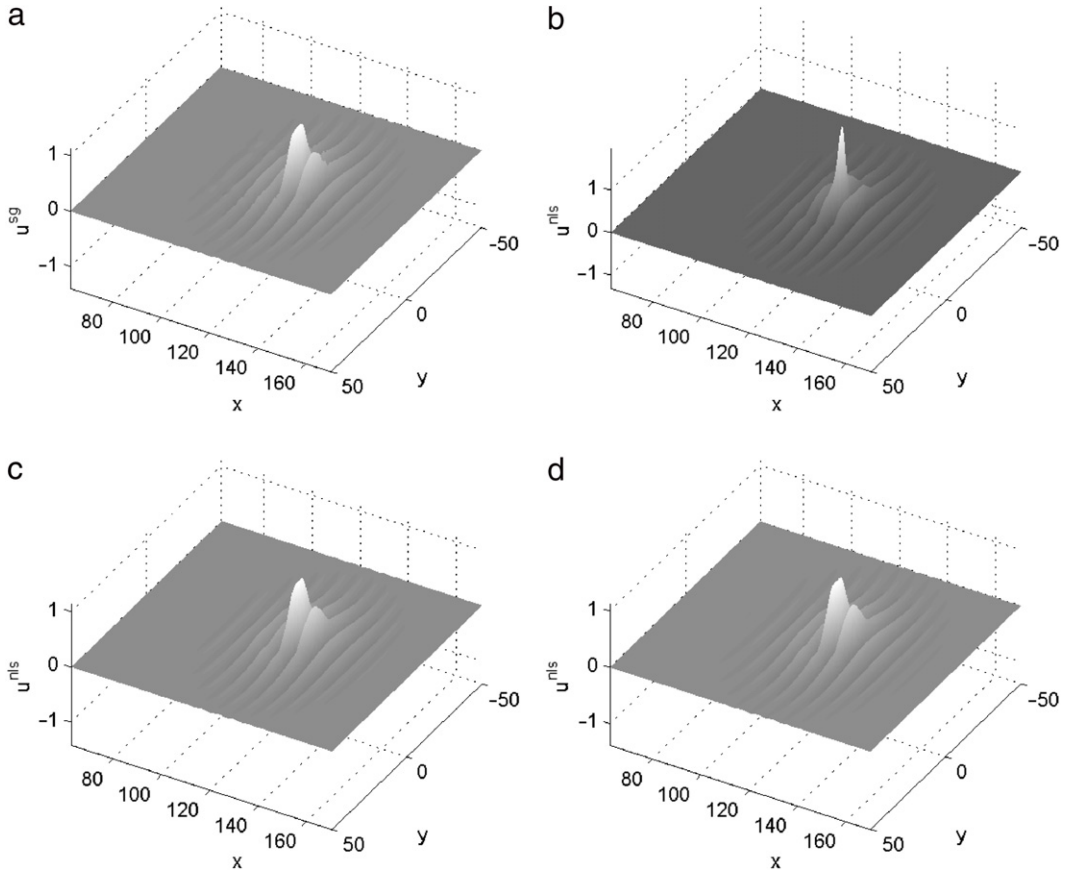

Fig. 6. Surface plots of the numerical solutions of u^{sg} and u^{nls} at $t = 179.2$ in the SG time scale which corresponds to $T = 0.1584 > T^*$ (after collapse of cubic NLS) in the NLS time scale for $\varepsilon = 0.05$ and $k = 1$. (a) SG solution; (b) perturbed NLS solution with $N = 0$; (c) perturbed NLS solution with $N = 1$; and (d) perturbed NLS solution with $N = 2$.

- *Numerical results well before collapse time of cubic NLS*, Fig. 2 shows the surface plots of u^{sg} of the SG equation (1.1) with $\varepsilon = 0.05$ and u^{nls} of the perturbed NLS equations with $N = 0, 1$ as well as cubic NLS at $t = 115.2$ in the SG time scale which corresponds to $T = 0.0950 < T^*$ in the NLS time scale (before collapse time of cubic NLS). The results for $\varepsilon = 0.1$ are similar and are omitted here for brevity. Fig. 3 plots u^{sg} and u^{nls} along the x-axis with $y = 0$ in this case.
- *Numerical results near collapse time of cubic NLS*, Fig. 4 shows the surface plots of u^{sg} of the SG equation (1.1) with $\varepsilon = 0.05$ and u^{nls} of the perturbed NLS equations with $N = 0, 1$ as well as cubic NLS at $t = 148.16$ in the SG time scales which corresponds to $T = 0.1310 \approx T^*$ in the NLS time scale (near collapse time of cubic NLS). We omit the similar results for $\varepsilon = 0.1$ here for brevity, and plot u^{sg} and u^{nls} along the x-axis with $y = 0$ in Fig. 5.
- *Numerical results well after collapse time of cubic NLS*, Fig. 6 shows the surface plots of u^{sg} of the SG equation (1.1) with $\varepsilon = 0.05$ and u^{nls} of the perturbed NLS equations with $N = 0, 1, 2$ at $t = 179.2$ in the SG time scale which corresponds to $T = 0.1584 > T^* >$ in the NLS time scale (after collapse time of cubic NLS). The similar results for $\varepsilon = 0.1$ are omitted here for brevity, and Fig. 7 plots u^{sg} and u^{nls} along the x-axis with $y = 0$ in this case.

We have also conducted simulations when cubic NLS dose not admit collapse in finite time, and the results are quite similar as before collapse time in the reported results above. From Figs. 2–7 and additional numerical results, for refined meshes, different ε as well as various k, not shown here for brevity, we can draw the following conclusions:

- In the time regime well before the collapse time of the cubic NLS, or cubic NLS without blow-up, both cubic NLS (2.13) and the perturbed NLS (2.10) with $N \geq 0$ agree qualitatively and quantitatively when ε reasonably small with the SG (1.1) for the propagation of light bullets (cf. Fig. 2).
- In the time regime near the collapse time of the cubic NLS, cubic NLS (2.13) fails to approximate the SG (1.1) quantitatively and qualitatively (cf. Figs. 4(a) & (b), 5 'top row'); the perturbed NLS (2.10) with $N \geq 0$ agrees qualitatively and quantitatively when ε reasonably small with the SG (1.1) (cf. Figs. 4(a), (c) & (d), and 5 'bottom row'), for the propagation of light bullets.
- In the time regime beyond the collapse time of the cubic NLS, cubic NLS (2.13) is no longer valid for the approximation of SG (1.1); the perturbed NLS (2.10) with $N = 0$ agrees qualitatively but not quantitatively with the SG (1.1) (cf. Figs. 6(a) & (b), 7 'top row'); and the perturbed NLS (2.10) with $N \geq 1$ agrees qualitatively and quantitatively when ε reasonably small with the SG (1.1) (cf. Figs. 6(a), (c) & (d), and 7 'bottom row'), for the propagation of light bullets.
- In general, for fixed time t, the smaller is the ε and the larger is N, the better is the approximation (cf. Figs. 3, 5 'bottom row', and 7 'bottom row').

The above observations validate what are normally expected, i.e., cubic NLS fails to match SG well before and beyond its collapse time, if any, but the perturbed NLS still agree with SG beyond the critical collapse.

4.2. Study on finite-term approximation

To understand how good the finite-term approximation (2.9) to (2.5) in the perturbed NLS (2.10) is, we solve (2.10) with the

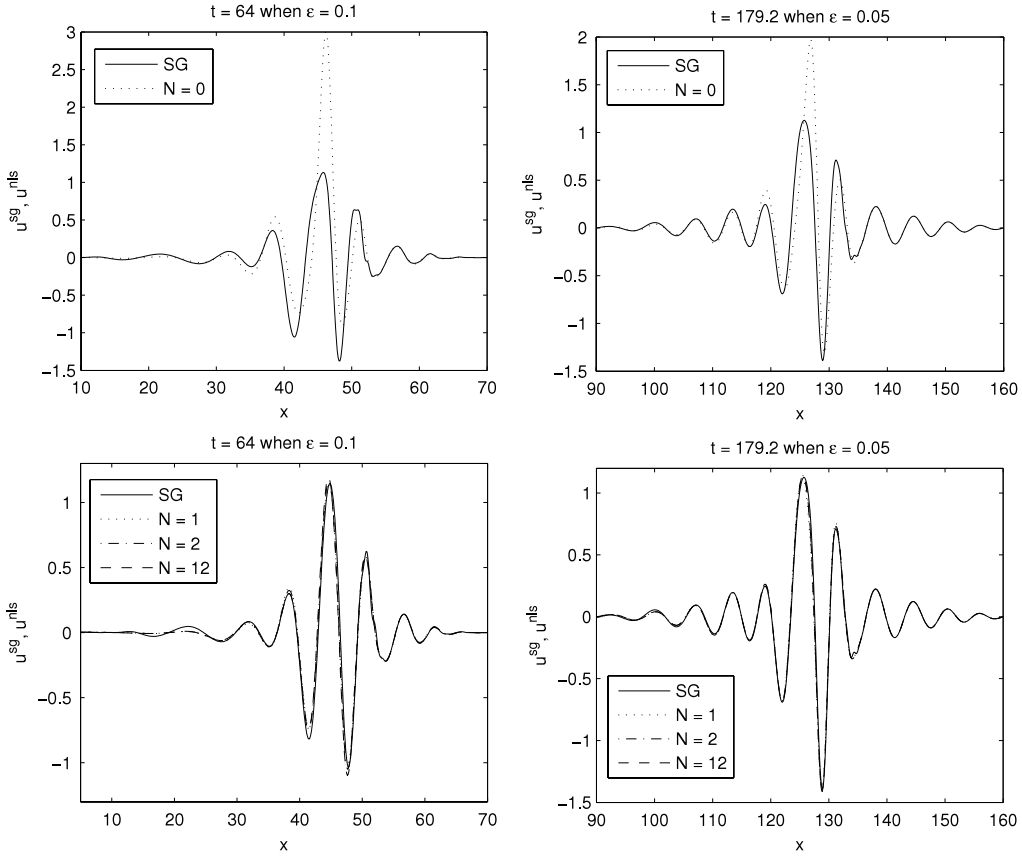

Fig. 7. Slice plots of the numerical solutions of u^{sg} and u^{nls} along x-axis with $y = 0$ for $k = 1$. Top row: comparison between SG and perturbed NLS with $N = 0$; Bottom row: comparison between SG and perturbed NLS with $N = 1, 2, 12$.

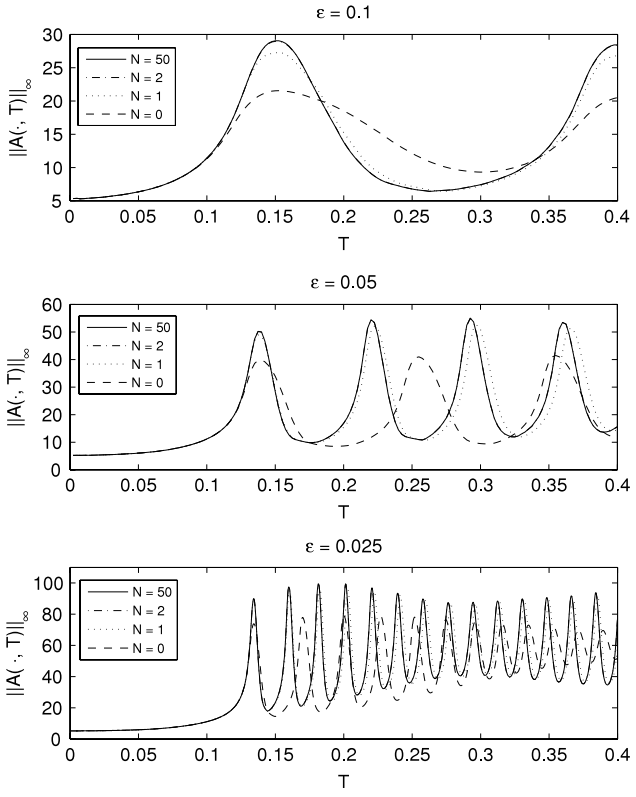

Fig. 8. Time evolution of $\|A(\mathbf{X}, T)\|_\infty$ for the perturbed NLS (2.10) with initial data (4.5) for different N and ε.

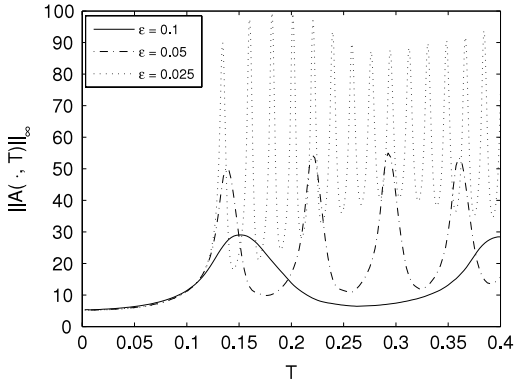

Fig. 9. Time evolution of $\|A(\mathbf{X}, T)\|_\infty$ for the perturbed NLS (2.10) with initial data (4.5) when $N = 50$ for different ε.

initial data (2.4) for different N and ε. Fig. 8 plots time evolution of $\|A(\mathbf{X}, T)\|_\infty$ when the initial data $A_0(\mathbf{X})$ in (2.4) is chosen as (4.5) with initial amplitude $a_0 = 5.2$, i.e., initial data leading to the occurrence of finite-time collapse in the cubic NLS, for different N and ε; and Fig. 9 shows similar results when $N = 50$ for different ε.

From Figs. 8 and 9 and additional numerical results, for different initial data in (2.4) and different ε and N, not shown here for brevity, we can draw the following conclusions: (i) For initial data in (2.4) when cubic NLS has no finite-time collapse, $\|A(\mathbf{X}, T)\|_\infty$ of either the cubic NLS (2.13) or the perturbed NLS (2.10) is uniformly bounded for $T \geq 0$, $N \geq 0$ and $0 < \varepsilon \leq \varepsilon_0$, for some ε_0. (ii) For initial data in (2.4) when cubic NLS has finite-time collapse, in the time regime $0 \leq T \leq T_0 < T^*$, i.e., well before the collapse time of cubic NLS, $\|A(\mathbf{X}, T)\|_\infty$ of the cubic NLS (2.13)

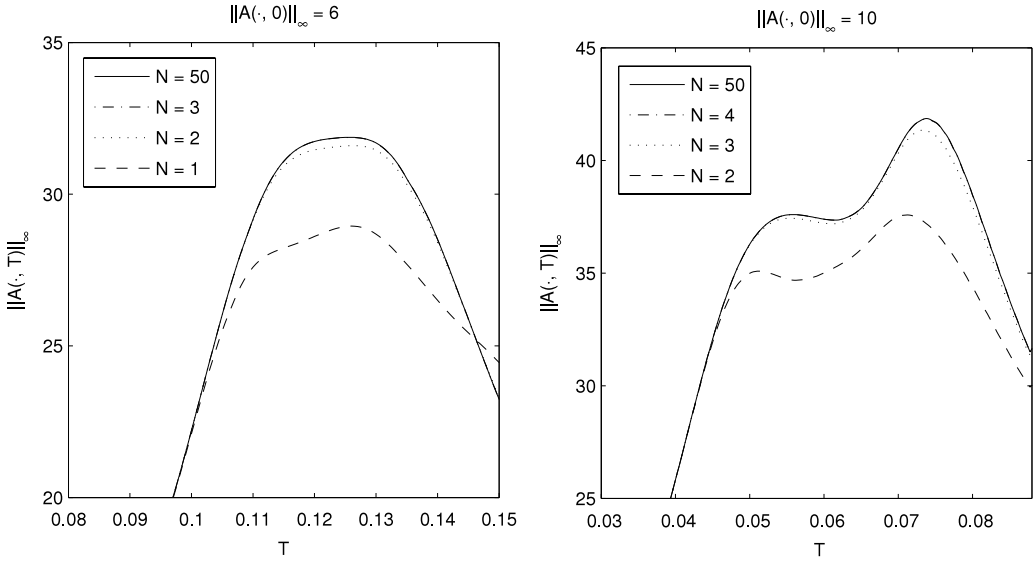

Fig. 10. Time evolution of $\|A(\mathbf{X}, T)\|_\infty$ for the perturbed NLS (2.10) with initial data (4.5) for different N and $\varepsilon = 0.1$.

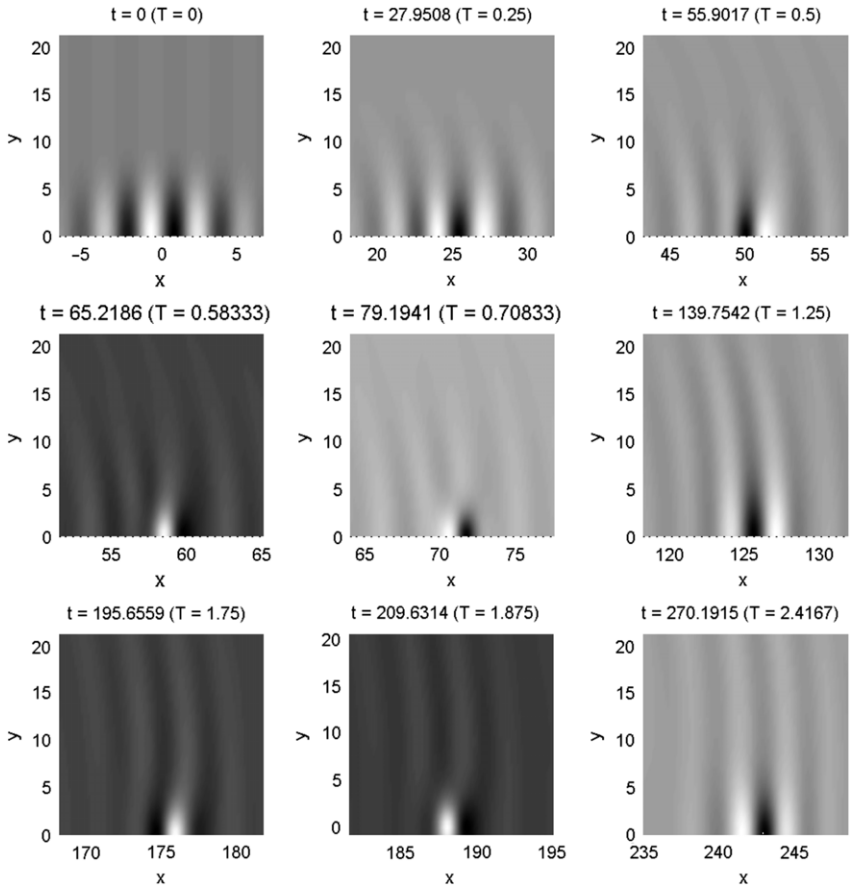

Fig. 11. Top view of u^{nls} in perturbed NLS (2.10) with reasonable large $N = 5$, for $\varepsilon = 0.2$ and initial data (4.8) with $a_0 = 3.5$ and $k = 2$: propagation far beyond critical NLS collapse time $T^* \approx 0.6980$.

and the perturbed NLS (2.10) is again uniformly bounded for $N \geq 0$ and $0 < \varepsilon \leq \varepsilon_0$; however, in the time regimes $T \approx T^*$ and $T > T^*$, i.e., near and after the collapse time of cubic NLS, $\|A(\mathbf{X}, T)\|_\infty$ of cubic NLS goes to ∞ when $T \to T^*$; for fixed $\varepsilon > 0$, $\|A(\mathbf{X}, T)\|_\infty$ of the perturbed NLS (2.10) is uniformly bounded for $N \geq 0$ and $T \geq T^*$ but the peak values of $\|A(\mathbf{X}, T)\|_\infty$ increases linearly as $O\left(\varepsilon^{-1}\right)$ (cf. Fig. 9) which implies $\varepsilon\|A(\mathbf{X}, T)\|_\infty$ is uniformly bounded (cf. Figs. 8 and 9), and such a bound depends on the initial amplitude. The linear increase of $\|A(\mathbf{X}, T)\|_\infty$ with ε^{-1} agrees with the modulation analysis of perturbed NLS. Recall from (5.4) of [6] that $|A(\mathbf{X}, T)| \sim L_\varepsilon^{-1} R$, where R is the bounded Townes soliton profile, and L_ε undergoes oscillation with minimum value of order $O(\varepsilon)$, see conclusion I(1) and (5.24) on p. 358 of [6]. It follows that in the regime of focusing–defocusing (breathing) cycle, $\|A(\mathbf{X}, T)\|_\infty = O(\varepsilon^{-1})$. (iii) When $N \geq N_0$ for some N_0, e.g. $N_0 = 3$ for the initial data (4.5), there is no substantial

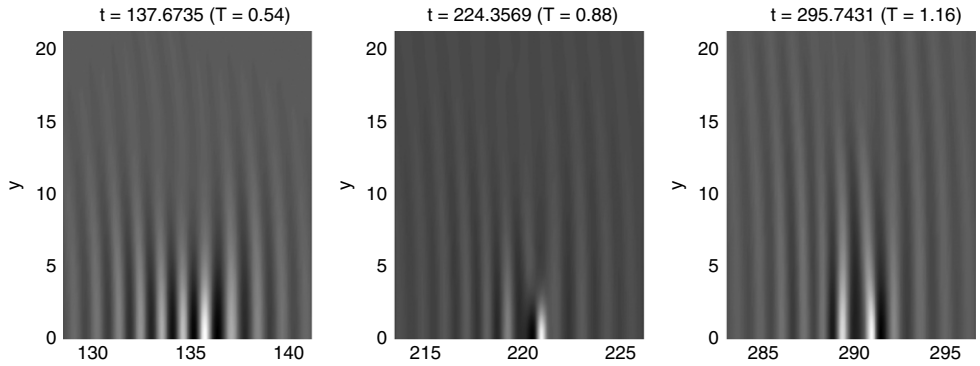

Fig. 12. Top view of u^{nls}, same parameters as Fig. 11, except that $k = 5$ and critical NLS collapse time is $T^* \approx 0.7280$.

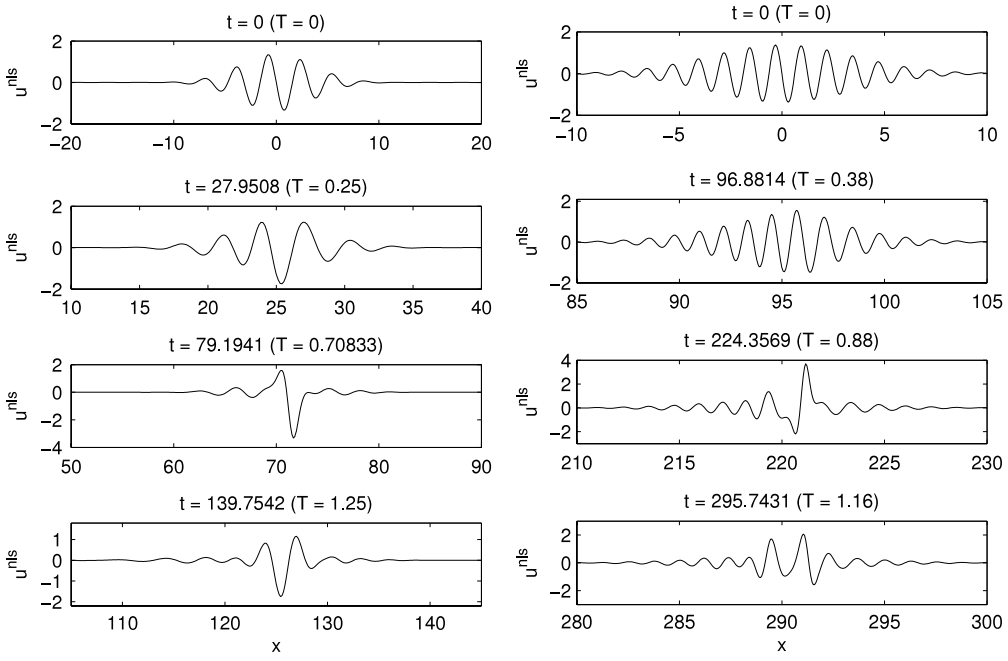

Fig. 13. Slice plots of u^{nls} along x-axis with $y = 0$: (1) left column, pulses in Fig. 11, i.e., $k = 2$; (2) right column, pulses in Fig. 12, i.e., $k = 5$.

difference in the dynamics of $\|A(\mathbf{X}, T)\|_\infty$ (cf. Fig. 8), and such an adequate N_0 also depends on initial amplitude (cf. Fig. 10). (iv) For fixed $N \geq 0$ and ε, the dynamics of $\|A(\mathbf{X}, T)\|_\infty$ shows focusing–defocusing cycles (cf. Fig. 8).

4.3. Propagation of light bullets in perturbed NLS

From the previous studies, we conclude that perturbed NLS (2.10) with reasonably large N (at this point we take $N = 5$ in the view of initial amplitude we use here) agrees with SG equation very well on modeling propagating pulses, also noticing that solving perturbed NLS requires much less computational load than SG equation due to the disparate scales involved and propagating property in SG light bullets solution; therefore, we shall solve the perturbed NLS here to study the propagation of light bullets instead of simulating SG equation. The initial data in (2.4) is chosen as

$$A^{(0)}(\mathbf{X}) = ia_0 \exp\left(-\frac{X^2}{\sigma_x^2} - \frac{Y^2}{\sigma_y^2}\right), \quad \mathbf{X} \in \mathbb{R}^2, \tag{4.8}$$

with $\sigma_x = \omega$ and $\sigma_y = 1$. Note that such initial data has been used extensively in previous studies [7,6] via solving SG equation directly. The below results are reported for $a_0 = 3.5$, $\varepsilon = 0.2$ and k is chosen as 2 or 5 respectively, and the results for other sets of parameters are quite similar and omitted here for brevity.

Fig. 11 presents the top view of pulse for $k = 2$, propagating far beyond the critical NLS collapse time and Fig. 12 depicts similarly for $k = 5$, which show that: (i) over time, the envelope tends to expand along y-axis slightly; (ii) before the collapse time the outside edge moves at a slower velocity than the centerline of the envelope; (iii) close to the collapse time, the envelope begins to destabilize (better observed in Figs. 13 and 5) and focus along x-axis, and the central part tends to delay, which can be explained by the focusing mechanism taking effect in the perturbed NLS or observed in the profile of solution A of perturbed NLS, and this phenomena can be also observed in Fig. 4; (iv) after the collapse time and before the focusing takes strong effect again in NLS, the envelope moves in a similar pattern as before collapse time, except that most pulse energy concentrates at the central part (cf. Fig. 13, where pulse profiles along x-axis are plotted, and also Fig. 7). Changing the envelope wave number k, we observe similar results.

5. Conclusion

We have compared numerically the solutions of the sine-Gordon (SG) equation, the perturbed nonlinear Schrödinger (NLS) equation, which is derived from the SG equation by carrying

out an envelope expansion, with its finite-term nonlinearity approximations, and the critical cubic NLS, for the propagation of light bullets in nonlinear optical media. This was achieved by the efficient semi-implicit sine pseudospectral methods, which are spectrally accurate in space, second order in time, and are very efficient in practical implementation. Based on our extensive numerical comparison results, we summarized the conclusions as follows, provided ε is reasonably small:

(i) If there is no finite-time collapse in the cubic NLS, then both cubic NLS and perturbed NLS agree with SG qualitatively and quantitatively.

(ii) If the cubic NLS collapses in finite time, then in the time regime well before the collapse time of the cubic NLS, both cubic NLS and perturbed NLS again agree with SG qualitatively and quantitatively; in the time regime near the collapse time of the cubic NLS, the cubic NLS fails to approximate the SG quantitatively and qualitatively where the perturbed NLS agrees with SG qualitatively and quantitatively; and in the time regime beyond the collapse time of the cubic NLS, the perturbed NLS with finite terms in the nonlinearity still agrees with SG qualitatively and quantitatively.

(iii) To well approximate the SG, the number of terms in the nonlinearity of the perturbed NLS depends on the initial data yet is independent of the small parameter ε. In general, only a few terms, e.g. $N \geq 3$, are needed in the perturbed NLS in practical computation.

Consequently, solving the perturbed NLS equations with reasonably many nonlinear terms demands much less computational load than simulating SG equation directly due to disparate scales involved. The computational domain for SG also needs to be adaptively extended if the propagation to a further time point is desired. Thus, the perturbed NLS is a more efficient model for numerically tracking the propagation of light bullets.

Acknowledgements

The authors acknowledge support from Ministry of Education of Singapore Grants R-146-000-120-112 and R-158-000-002-112 and the US NSF Grant DMS-0712881. This work was initiated when W.B. was on his sabbatical leave in 2008 at Department of Mathematics, University of California at Irvine and he would like to thank his host Professors Jack Xin and John Lowengrub for their warm hospitality and support. Also, the authors thank the anonymous referees for their constructive comments and helpful suggestions on the early manuscript.

Appendix A. Proof of the Theorem 3.1

From the regularity of the solution, we have

$$\max_{0\leq t\leq t^*}\left\{\left\|\partial_t^4 u(\cdot,t)\right\|_{L^2},\left\|\partial_t^3 u(\cdot,t)\right\|_{H^1},\left\|\partial_{tt} u(\cdot,t)\right\|_{H^2},\ \|u(\cdot,t)\|_{H^m}\right\}\lesssim 1. \tag{A.1}$$

Denote

$$u_{JK}(\mathbf{x},t_n) := P_{JK}u(\mathbf{x},t_n),$$
$$\eta^n(\mathbf{x}) := u_{JK}(\mathbf{x},t_n) - u_{JK}^n(\mathbf{x}),\quad \mathbf{x}\in\Omega,\ n\geq 0, \tag{A.2}$$

then $\eta^n(\mathbf{x})\in Y_{JK}$, and define the local truncation errors

$$\begin{aligned}\tau^0(\mathbf{x}) &= \frac{u(\mathbf{x},t_1)-u^{(0)}(\mathbf{x})}{\Delta t} - u^{(1)}(\mathbf{x})\\ &\quad -\frac{\Delta t}{2}\left[c^2\nabla^2 u^{(0)}(\mathbf{x}) - \sin\left(u^{(0)}(\mathbf{x})\right)\right],\end{aligned} \tag{A.3}$$

$$\begin{aligned}\tau^n(\mathbf{x}) &= \frac{u(\mathbf{x},t_{n+1})-2u(\mathbf{x},t_n)+u(\mathbf{x},t_{n-1})}{(\Delta t)^2}\\ &\quad -\frac{c^2}{2}\left[\nabla^2 u(\mathbf{x},t_{n+1})+\nabla^2 u(\mathbf{x},t_{n-1})\right]\\ &\quad +\sin(u(\mathbf{x},t_n)),\quad 1\leq n\leq \frac{t^*}{\Delta t}-1,\ \mathbf{x}\in\Omega.\end{aligned} \tag{A.4}$$

Applying Taylor expansions to (A.3), noticing (1.1), (1.2) and (A.1), using Hölder inequality, we get

$$\begin{aligned}\|\tau^0\|_{L^2}^2 &= \int_\Omega\left[\int_0^{\Delta t}\frac{t^2}{2(\Delta t)}\partial_t^3 u(\mathbf{x},t)\mathrm{d}t\right]^2\mathrm{d}\mathbf{x}\\ &\leq \int_\Omega\left[\int_0^{\Delta t}\frac{t^4}{4(\Delta t)^2}\mathrm{d}t\cdot\int_0^{\Delta t}\left|\partial_t^3 u(\mathbf{x},t)\right|^2\mathrm{d}t\right]\mathrm{d}\mathbf{x}\\ &\leq \frac{(\Delta t)^3}{20}\int_0^{\Delta t}\int_\Omega\left|\partial_t^3 u(\mathbf{x},t)\right|^2\mathrm{d}\mathbf{x}\mathrm{d}t\\ &= \frac{(\Delta t)^3}{20}\int_0^{\Delta t}\|\partial_t^3 u(\cdot,t)\|_{L^2}^2\mathrm{d}t\\ &\leq \frac{(\Delta t)^4}{20}\max_{0\leq t\leq\Delta t}\|\partial_t^3 u(\cdot,t)\|_{L^2}^2\lesssim(\Delta t)^4.\end{aligned} \tag{A.5}$$

Similarly, we have

$$\|\nabla\tau^0\|_{L^2}^2 = \int_\Omega\left[\int_0^{\Delta t}\frac{t^2}{2(\Delta t)}\partial_t^3\nabla u(\mathbf{x},t)\mathrm{d}t\right]^2\mathrm{d}\mathbf{x}\lesssim(\Delta t)^4. \tag{A.6}$$

From (A.4), (1.1) and (A.1), we obtain

$$\begin{aligned}\|\tau^n\|_{L^2}^2 &\leq \int_\Omega\left\{\int_{t_n}^{t_{n+1}}\left[\frac{(t-t_n)^3}{12(\Delta t)^2}\partial_t^4 u(\mathbf{x},t)\right.\right.\\ &\quad\left.+\frac{c^2}{2}(t-t_n)\partial_t^2\nabla^2 u(\mathbf{x},t)\right]\mathrm{d}t\\ &\quad+\int_{t_{n-1}}^{t_n}\left[\frac{(t_n-t)^3}{12(\Delta t)^2}\partial_t^4 u(\mathbf{x},t)\right.\\ &\quad\left.\left.+\frac{c^2}{2}(t_n-t)\partial_t^2\nabla^2 u(\mathbf{x},t)\right]\mathrm{d}t\right\}^2\mathrm{d}\mathbf{x}\\ &\leq (\Delta t)^4\left[\frac{1}{126}\max_{t_{n-1}\leq t\leq t_{n+1}}\|\partial_t^4 u(\cdot,t)\|_{L^2}^2\right.\\ &\quad\left.+\frac{2c^4}{3}\max_{t_{n-1}\leq t\leq t_{n+1}}\|\partial_t^2\nabla^2 u(\cdot,t)\|_{L^2}^2\right]\\ &\lesssim (\Delta t)^4,\quad 1\leq n\leq\frac{t^*}{\Delta t}-1.\end{aligned} \tag{A.7}$$

Applying the projection operator P_{JK} to (A.3) and (A.4), noticing (A.2), we obtain

$$\begin{aligned}P_{JK}\tau^0(\mathbf{x}) &= \frac{u_{JK}(\mathbf{x},t_1)-u_{JK}^0}{\Delta t} - P_{JK}u^{(1)}\\ &\quad -\frac{\Delta t}{2}\left[c^2\nabla^2 u_{JK}^0 - P_{JK}\sin\left(u^{(0)}\right)\right],\end{aligned} \tag{A.8}$$

$$\begin{aligned}P_{JK}\tau^n(\mathbf{x}) &= \frac{u_{JK}(\mathbf{x},t_{n+1})-2u_{JK}(\mathbf{x},t_n)+u_{JK}(\mathbf{x},t_{n-1})}{(\Delta t)^2}\\ &\quad +P_{JK}\sin(u(\mathbf{x},t_n)) - \frac{c^2}{2}\left[\nabla^2 u_{JK}(\mathbf{x},t_{n+1})+\nabla^2 u_{JK}(\mathbf{x},t_{n-1})\right],\\ &\quad \mathbf{x}\in\Omega,\ 1\leq n\leq\frac{t^*}{\Delta t}-1.\end{aligned} \tag{A.9}$$

Subtracting (3.5) and (3.6) from (A.9) and (A.8), respectively, noting (A.2), we have for $1\leq n\leq\frac{t^*}{\Delta t}-1$,

$$\frac{\eta^{n+1}(\mathbf{x})-2\eta^{n}(\mathbf{x})+\eta^{n-1}(\mathbf{x})}{(\Delta t)^2}-\frac{c^2}{2}\left[\nabla^2\eta^{n+1}(\mathbf{x})+\nabla^2\eta^{n-1}(\mathbf{x})\right]$$
$$=g^n(\mathbf{x})-P_{JK}(\tau^n(\mathbf{x})), \tag{A.10}$$

$$\eta^0(\mathbf{x})=0,\qquad \frac{\eta^1(\mathbf{x})-\eta^0(\mathbf{x})}{\Delta t}=P_{JK}(\tau^0(\mathbf{x})),\quad \mathbf{x}\in\Omega, \tag{A.11}$$

where,

$$g^n(\mathbf{x})=P_{JK}\left[\sin\left(u_{JK}^n\right)-\sin(u(\mathbf{x},t_n))\right],$$
$$\mathbf{x}\in\Omega,\ 1\le n\le\frac{t^*}{\Delta t}. \tag{A.12}$$

From (A.12), using Poincaré inequality, we get

$$\begin{aligned}\left\|g^n\right\|_{L^2}&\le\left\|\sin\left(u_{JK}^n(\mathbf{x})\right)-\sin(u(\mathbf{x},t_n))\right\|_{L^2}\\&\le\|\cos(\cdot)\|_{L^\infty}\cdot\left\|u_{JK}^n(\mathbf{x})-u(\mathbf{x},t_n)\right\|_{L^2}\\&\le\left\|\mathrm{e}^n\right\|_{L^2}\le\|\eta^n\|_{L^2}+\|u(\mathbf{x},t_n)-P_{JK}u(\mathbf{x},t_n)\|_{L^2}\\&\lesssim\|\nabla\eta^n\|_{L^2}+h^m,\quad 1\le n\le\frac{t^*}{\Delta t}.\end{aligned} \tag{A.13}$$

Define the energy for the error function η^n as

$$\mathcal{E}^n=\left\|\frac{\eta^{n+1}-\eta^n}{\Delta t}\right\|_{L^2}^2+\frac{c^2}{2}\left(\left\|\nabla\eta^{n+1}\right\|_{L^2}^2+\left\|\nabla\eta^n\right\|_{L^2}^2\right),$$
$$0\le n\le\frac{t^*}{\Delta t}-1. \tag{A.14}$$

Using (A.11), (A.5) and (A.6), we have

$$\left\|\frac{\eta^1-\eta^0}{\Delta t}\right\|_{L^2}^2\le\|P_{JK}(\tau^0)\|_{L^2}^2\le\|\tau^0\|_{L^2}^2\lesssim(\Delta t)^4, \tag{A.15a}$$
$$\|\nabla\eta^0\|_{L^2}^2=0,$$
$$\|\nabla\eta^1\|_{L^2}^2=(\Delta t)^2\|P_{JK}(\nabla\tau^0)\|_{L^2}^2\le(\Delta t)^2\|\nabla\tau^0\|_{L^2}^2\lesssim(\Delta t)^6. \tag{A.15b}$$

Plugging (A.15a) and (A.15b) into (A.14) with $n=0$, we get

$$\mathcal{E}^0\lesssim(1+(\Delta t)^2)(\Delta t)^4. \tag{A.16}$$

Multiplying both sides of (A.10) by $\eta^{n+1}-\eta^{n-1}$, and integrating over Ω and using integration by parts, noticing (A.14), (A.7) and (A.13), we have

$$\begin{aligned}\mathcal{E}^n-\mathcal{E}^{n-1}&\le\int_\Omega\left(|P_{JK}(\tau^n)|+|g^n|\right)\left|\eta^{n+1}-\eta^{n-1}\right|\mathrm{d}\mathbf{x},\\&=\Delta t\int_\Omega\left(|P_{JK}(\tau^n)|+|g^n|\right)\left|\frac{\eta^{n+1}-\eta^n}{\Delta t}+\frac{\eta^n-\eta^{n-1}}{\Delta t}\right|\mathrm{d}\mathbf{x}\\&\le\Delta t\left[\left\|P_{JK}(\tau^n)\right\|_{L^2}^2+\left\|g^n\right\|_{L^2}^2\right.\\&\quad\left.+\left\|\frac{\eta^{n+1}-\eta^n}{\Delta t}\right\|_{L^2}^2+\left\|\frac{\eta^n-\eta^{n-1}}{\Delta t}\right\|_{L^2}^2\right]\\&\lesssim\Delta t\left[(\Delta t)^4+h^{2m}+\mathcal{E}^n+\mathcal{E}^{n-1}\right],\quad 1\le n\le\frac{t^*}{\Delta t}-1.\end{aligned} \tag{A.17}$$

Then, there exists a positive constant $k_0\le 1$, such that for $0<\Delta t\le k_0$,

$$\mathcal{E}^n-\mathcal{E}^{n-1}\lesssim\Delta t\left[(\Delta t)^4+h^{2m}+\mathcal{E}^{n-1}\right],$$
$$1\le n\le\frac{t^*}{\Delta t}-1. \tag{A.18}$$

Summing up for $n\ge 1$, and noticing (A.16), we obtain

$$\mathcal{E}^n\lesssim(\Delta t)^4+h^{2m}+\Delta t\sum_{r=0}^{n-1}\mathcal{E}^r,\quad 1\le n\le\frac{t^*}{\Delta t}-1. \tag{A.19}$$

Using the discrete Gronwall's inequality, we obtain

$$\mathcal{E}^n\lesssim(\Delta t)^4+h^{2m},\quad 0\le n\le\frac{t^*}{\Delta t}-1. \tag{A.20}$$

Thus the desired result (3.7) follows from (A.20) and (A.14) as well as the following triangle inequality

$$\begin{aligned}\|\nabla\mathrm{e}^n\|_{L^2}&\le\|\nabla\eta^n\|_{L^2}+\|\nabla\left(u(\mathbf{x},t_n)-P_{JK}u(\mathbf{x},t_n)\right)\|_{L^2}\\&\lesssim\|\nabla\eta^n\|_{L^2}+h^{m-1},\quad 0\le n\le\frac{t^*}{\Delta t}.\end{aligned}$$

Appendix B. Proof of the Theorem 3.2

The proof proceeds in mathematical induction, and without loss of generality, we assume $\Delta X=\Delta Y$ and $\kappa=1$, i.e., $\Delta T\le h$. From the regularity of the solution, we have

$$\max_{0\le T\le T^*}\left\{\left\|\partial_T^4A(\mathbf{X},T)\right\|_{L^2},\left\|\partial_T^3A(\mathbf{X},T)\right\|_{H^1},\right.$$
$$\left.\|\partial_{TT}A(\mathbf{X},T)\|_{H^2},\|A(\mathbf{X},T)\|_{H^m},\|A(\mathbf{X},T)\|_{L^\infty}\right\}\lesssim 1, \tag{B.1}$$

and by the smoothness of f_ε^N,

$$\max_{0\le T\le T^*}\left\{\left\|f_\varepsilon^N\left(|A(\mathbf{X},T)|^2\right)\right\|_{L^\infty},\right.$$
$$\left.\left\|\left(f_\varepsilon^N\right)'\left((|A(\mathbf{X},T)|+1)^2\right)\right\|_{L^\infty}\right\}\lesssim 1. \tag{B.2}$$

Denote

$$A_{JK}(\mathbf{X},T_n):=P_{JK}A(\mathbf{X},T_n),$$
$$\eta^n(\mathbf{X}):=A_{JK}(\mathbf{X},T_n)-A_{JK}^n(\mathbf{X}),\quad \mathbf{X}\in\Omega,\ n\ge 0, \tag{B.3}$$

then $\eta^n(\mathbf{X})\in Y_{JK}$, and define the local truncation errors as

$$\begin{aligned}\tau^0(\mathbf{X})&=\frac{A(\mathbf{X},T_1)-A^{(0)}(\mathbf{X})}{\Delta T}-A^{(1)}(\mathbf{X})\\&\quad-\frac{4\omega^2\Delta T}{2\varepsilon^2}\left[\mathrm{i}A^{(1)}(\mathbf{X})+\nabla^2A^{(0)}(\mathbf{X})+\frac{\varepsilon ck}{\omega}\partial_XA^{(1)}(\mathbf{X})\right.\\&\quad\left.-P_{JK}\left(f_\varepsilon^N\left(|A^{(0)}(\mathbf{X})|^2\right)A^{(0)}(\mathbf{X})\right)\right],\quad\mathbf{X}\in\Omega,\end{aligned} \tag{B.4}$$

$$\begin{aligned}\tau^n(\mathbf{X})&=\mathrm{i}\frac{A(\mathbf{X},T_{n+1})-A(\mathbf{X},T_{n-1})}{2\Delta T}\\&\quad-\frac{\varepsilon^2}{4\omega^2}\frac{A(\mathbf{X},T_{n+1})-2A(\mathbf{X},T_n)+A(\mathbf{X},T_{n-1})}{(\Delta T)^2}\\&\quad+\frac{1}{2}\left(\nabla^2A(\mathbf{X},T_{n+1})+\nabla^2A(\mathbf{X},T_{n-1})\right)\\&\quad-f_\varepsilon^N\left(|A(\mathbf{X},T_n)|^2\right)A(\mathbf{X},T_n)+\frac{\varepsilon ck}{2\omega\Delta T}\Big(\partial_XA(\mathbf{X},T_{n+1})\\&\quad-\partial_XA(\mathbf{X},T_{n-1})\Big),\quad 1\le n\le\frac{T^*}{\Delta T}-1,\end{aligned} \tag{B.5}$$

then via similar arguments as (A.5)–(A.7), we get

$$\left\|\tau^n\right\|_{L^2}^2\lesssim(\Delta T)^4,\quad 0\le n\le\frac{T^*}{\Delta T}-1,$$
$$\left\|\nabla\tau^0\right\|_{L^2}^2\lesssim(\Delta T)^4. \tag{B.6}$$

Similar with Theorem 3.1, the error function η^n satisfies,

$$\mathrm{i}\frac{\eta^{n+1}(\mathbf{X})-\eta^{n-1}(\mathbf{X})}{2\Delta T}=\frac{\varepsilon^2}{4\omega^2}\frac{\eta^{n+1}(\mathbf{X})-2\eta^n(\mathbf{X})+\eta^{n-1}(\mathbf{X})}{(\Delta T)^2}$$
$$-\frac{\varepsilon ck}{2\omega\Delta T}\left(\partial_X\eta^{n+1}(\mathbf{X})-\partial_X\eta^{n-1}(\mathbf{X})\right)-\frac{1}{2}\left(\nabla^2\eta^{n+1}(\mathbf{X})\right.$$

$$+\nabla^2\eta^{n-1}(\mathbf{X})\big)+q^n(\mathbf{X})+P_{JK}\left(\tau^n(\mathbf{X})\right),$$
$$1\le n\le\frac{T^*}{\Delta T}-1, \tag{B.7}$$
$$\eta^0(\mathbf{X})=0,\qquad \frac{\eta^1(\mathbf{X})-\eta^0}{\Delta T}=P_{JK}\left(\tau^0(\mathbf{X})\right),\quad \mathbf{X}\in\Omega, \tag{B.8}$$

where for $1\le n\le T^*/\Delta T-1$,

$$q^n(\mathbf{X})=P_{JK}\big[f_\varepsilon^N\left(|A(\mathbf{X},T_n)|^2\right)A(\mathbf{X},T_n) -f_\varepsilon^N\left(|A_{JK}^n(\mathbf{X})|^2\right)A_{JK}^n(\mathbf{X})\big]. \tag{B.9}$$

Define the energy for error function η^n as

$$\mathcal{E}^n=\frac{\varepsilon^2}{4\omega^2}\left\|\frac{\eta^{n+1}-\eta^n}{\Delta T}\right\|_{L^2}^2 +\frac{1}{2}\left(\left\|\nabla\eta^{n+1}\right\|_{L^2}^2+\left\|\nabla\eta^n\right\|_{L^2}^2\right),\quad 0\le n\le\frac{T^*}{\Delta T}-1. \tag{B.10}$$

Then, similar as (A.15a), (A.15b) and (A.16), we have,

$$\mathcal{E}^0\lesssim\left(1+(\Delta T)^2\right)(\Delta T)^4. \tag{B.11}$$

Multiplying both sides of (B.7) by $\overline{\eta^{n+1}}-\overline{\eta^{n-1}}$, integrating over Ω and taking the real part, with similar argument as (A.17), we have for $1\le n\le T^*/\Delta T-1$,

$$\mathcal{E}^n-\mathcal{E}^{n-1}\le\Delta T\Bigg[\left\|q^n\right\|_{L^2}^2+\left\|P_{JK}\left(\tau^n\right)\right\|_{L^2}^2 +\left\|\frac{\eta^{n+1}-\eta^n}{\Delta T}\right\|_{L^2}^2+\left\|\frac{\eta^n-\eta^{n-1}}{\Delta T}\right\|_{L^2}^2\Bigg]. \tag{B.12}$$

Note that

$$\left\|\eta^1\right\|_{L^2}=\Delta T\left\|P_{JK}(\tau^0)\right\|_{L^2}\lesssim(\Delta T)^3,$$
$$\left\|\nabla\eta^1\right\|_{L^2}=\Delta T\left\|P_{JK}(\nabla\tau^0)\right\|_{L^2}\lesssim(\Delta T)^3,$$

then,

$$\left\|\mathrm{e}^1\right\|_{L^2}\le\left\|\eta^1\right\|_{L^2}+\left\|P_{JK}A(\mathbf{X},T_1)-A(\mathbf{X},T_1)\right\|_{L^2}\lesssim(\Delta T)^3+h^m,$$
$$\left\|\nabla\mathrm{e}^1\right\|_{L^2}\lesssim\left\|\nabla\eta^1\right\|_{L^2}+\left\|\nabla\left(P_{JK}A(\mathbf{X},T_1)-A(\mathbf{X},T_1)\right)\right\|_{L^2} \lesssim(\Delta T)^3+h^{m-1}, \tag{B.13}$$

which results in the estimate (3.12) for $n=1$.

Since $\eta^n\in Y_{JK}$ and noticing $\Delta T\le h$, we have

$$\left\|\eta^1\right\|_{L^\infty}\lesssim\frac{1}{h}\left\|\eta^1\right\|_{L^2}\lesssim(\Delta T)^2, \tag{B.14}$$

and then,

$$\left\|\mathrm{e}^1\right\|_{L^\infty}\le\left\|\eta^1\right\|_{L^\infty}+\left\|P_{JK}A(\mathbf{X},T_1)-A(\mathbf{X},T_1)\right\|_{L^\infty} \le C_1\left((\Delta T)^2+h^m\right). \tag{B.15}$$

Choose $k_0'>0$ and $h_0'>0$ such that

$$C_1\left((k_0')^2+(h_0')^m\right)\le 1, \tag{B.16}$$

i.e.,

$$\left\|A_{JK}^1\right\|_{L^\infty}\le\|A(\mathbf{X},T_1)\|_{L^\infty}+\left\|\mathrm{e}^1\right\|_{L^\infty}\le\|A(\mathbf{X},T_1)\|_{L^\infty}+1, \quad \Delta T\le k_0',\quad h\le h_0'. \tag{B.17}$$

Now we estimate $\mathcal{E}^1$. At $T=T_1$, noticing (B.2) and (B.17), we have,

$$\begin{aligned}\left\|q^1\right\|_{L^2}&\le\left\|f_\varepsilon^N(|A(\mathbf{X},T_1)|^2)A(\mathbf{X},T_1)-f_\varepsilon^N(|A_{JK}^1|^2)A_{JK}^1\right\|_{L^2}\\ &\le\left\|f_\varepsilon^N(|A(\mathbf{X},T_1)|^2)\right\|_{L^\infty}\left\|\mathrm{e}^1\right\|_{L^2}\\ &\quad+\left\|\left(f_\varepsilon^N\left(|A(\mathbf{X},T_1)|^2\right)-f_\varepsilon^N\left(|A_{JK}^1|^2\right)\right)A_{JK}^1\right\|_{L^2}\\ &\lesssim\left\|\mathrm{e}^1\right\|_{L^2}\Big[1+(2\|A(\mathbf{X},T_1)\|_{L^\infty}+1)^2\\ &\quad\times\left\|(f_\varepsilon^N)'\left((|A(\mathbf{X},T_1)|+1)^2\right)\right\|_{L^\infty}\Big]\\ &\lesssim\left\|\mathrm{e}^1\right\|_{L^2}\lesssim\|\eta^1\|_{L^2}+h^m\le C_2\left(\|\nabla\eta^1\|_{L^2}+h^m\right).\end{aligned} \tag{B.18}$$

Plugging (B.6) and (B.18) into (B.12) and noticing (B.10), we obtain,

$$\mathcal{E}^1-\mathcal{E}^0\le C_3\Delta T\left[(\Delta T)^4+h^{2m}+\left(\mathcal{E}^1+\mathcal{E}^0\right)\right]. \tag{B.19}$$

Then when $\Delta T\le\frac{1}{2C_3}$, we have

$$\mathcal{E}^1\le\mathcal{E}^0+4C_3\Delta T\left[(\Delta T)^4+h^{2m}+\mathcal{E}^0\right]. \tag{B.20}$$

Then, noticing the estimate of $\mathcal{E}^0$ (B.11), for $h\le h_0'$ and $\Delta T\le\min\left\{\frac{1}{2C_3},k_0'\right\}$, we have

$$\begin{aligned}\mathcal{E}^1&\le(C_4+4C_3\Delta T)\left((\Delta T)^4+h^{2m}\right)\mathrm{e}^{4C_3\Delta T}\\ &\le(C_4+4C_3T^*)\left((\Delta T)^4+h^{2m}\right)\mathrm{e}^{4C_3T^*}\\ &:=C_5\left((\Delta T)^4+h^{2m}\right).\end{aligned} \tag{B.21}$$

In the view of (B.10) for $n=1$, with the above estimate on $\mathcal{E}^1$, we have,

$$\left\|\eta^2\right\|_{L^2}\lesssim\left\|\nabla\eta^2\right\|_{L^2}\lesssim(\Delta T)^2+h^m,$$
$$\left\|\eta^2\right\|_{L^\infty}\lesssim\frac{1}{h}\left\|\eta^2\right\|_{L^2}\lesssim\Delta T+h^{m-1}. \tag{B.22}$$

So,

$$\left\|\mathrm{e}^2\right\|_{L^2}\lesssim(\Delta T)^2+h^m,\qquad\left\|\nabla\mathrm{e}^2\right\|_{L^2}\lesssim(\Delta T)^2+h^{m-1},$$
$$\left\|\mathrm{e}^2\right\|_{L^\infty}\le C_6(\Delta T+h^{m-1}), \tag{B.23}$$

which establishes (3.12) for $n=2$. Note, there exist $k_0''>0$ and $h_0''>0$, such that

$$C_6((k_0'')+(h_0'')^{m-1})\le 1, \tag{B.24}$$

and so $\left\|\mathrm{e}^2\right\|_{L^\infty}\le 1$ if $\Delta T\le k_0''$ and $h\le h_0''$.

We choose,

$$k_0=\min\left\{\frac{1}{2C_3},k_0',k_0''\right\},\qquad h_0=\min\{h_0',h_0''\}, \tag{B.25}$$

where k_0' and h_0' are chosen so as to (B.16) holds, and k_0'' and h_0'' are chosen such that (B.24) is valid. Noting that k_0 and h_0 only depend on the regularity of solution and smoothness of f_ε^N, i.e., (B.1) and (B.2), as well as the final computation time T^*, the rest justification is due to induction.

For $1\le n\le T^*/\Delta T-1$ and $\Delta T\le k_0$ and $h\le h_0$, satisfying $\Delta T\le h$, we assume,

$$\left\|\mathrm{e}^l\right\|_{L^2}\lesssim(\Delta T)^2+h^m,\qquad\left\|\nabla\mathrm{e}^l\right\|_{L^2}\lesssim(\Delta T)^2+h^{m-1},$$
$$\left\|\mathrm{e}^l\right\|_{L^\infty}\le 1,\quad 2\le l\le n, \tag{B.26}$$

and for $l=1$, we already have (B.13) and (B.17), then

$$\left\|A_{JK}^l(\mathbf{X})\right\|_{L^\infty}\le\|A(\mathbf{X},T_l)\|_{L^\infty}+1,\quad 1\le l\le n. \tag{B.27}$$

With similar argument as (B.18) we have,

$$\left\|q^l\right\|_{L^2}\le C_2\left(\left\|\nabla\eta^l\right\|_{L^2}+h^m\right),\quad 1\le l\le n. \tag{B.28}$$

Noticing (B.12) and (B.6), similar as proof of Theorem 3.1, when $\Delta T \le \frac{1}{2C_3}$, we have,

$$\mathcal{E}^n \le \mathcal{E}^0 + 4C_3 n\Delta T\left[(\Delta T)^4 + h^{2m}\right] + 4C_3\Delta T\sum_{l=0}^{n-1}\mathcal{E}^l. \tag{B.29}$$

Since $n \le T^*/\Delta T - 1$, when $\Delta T \le \min\left\{\frac{1}{2C_3}, k_0'\right\}$, we obtain by using discrete Gronwall's inequality and noting (B.11),

$$\mathcal{E}^n \le (C_4 + 4C_3 n\Delta T)\left((\Delta T)^4 + h^{2m}\right) \le C_5\left((\Delta T)^4 + h^{2m}\right). \tag{B.30}$$

In the view of (B.10), similar as (B.22) and (B.23), we obtain

$$\left\|e^{n+1}\right\|_{L^2} \lesssim (\Delta T)^2 + h^m, \qquad \left\|\nabla e^{n+1}\right\|_{L^2} \lesssim (\Delta T)^2 + h^{m-1},$$
$$\left\|e^{n+1}\right\|_{L^\infty} \le C_6\left(\Delta T + h^{m-1}\right). \tag{B.31}$$

Noticing k_0 and h_0 are chosen as (B.25), when $\Delta T \le k_0$ and $h \le h_0$, we have,

$$\left\|e^{n+1}\right\|_{L^\infty} \le 1. \tag{B.32}$$

In above estimates, the constants $C_1, C_2, \ldots, C_6$ are the same as those in (B.18)–(B.23) and they are independent of mesh size h and time step ΔT as well as time steps $0 \le n \le \frac{T}{\Delta T}$, therefore k_0', k_0'', h_0' and h_0'' are the same as before and they can be chosen such that they are independent of mesh size h and time step ΔT as well as time steps $0 \le n \le \frac{T}{\Delta T}$ too. Hence, (B.31) and (B.32) prove (B.26) for $l = n+1$, and the claim in Theorem 3.2 follows by mathematical induction. □

References

[1] G.P. Agrawal, Nonlinear Fiber Optics, Academic Press, New York, 1989.
[2] A. Hasegawa, Optical Solitons in Fibers, Springer, New York, 1989.
[3] P. Goorjian, Y. Silberberg, Numerical simulations of light bullets using the full-vector time-dependent nonlinear Maxwel equations, J. Opt. Soc. Amer. B Opt. Phys. 14 (1997) 3253–3260.
[4] C.V. Hile, Comparisons between Maxwell's equations and an extended nonlinear Schrödinger equation, Wave Motion 24 (1996) 1–12.
[5] C.V. Hile, W.L. Kath, Numerical solutions of Maxwell's equations for nonlinear optical pulse propagation, J. Opt. Soc. Amer. B 13 (1996) 1135–1146.
[6] J. Xin, Modeling light bullets with the two-dimensional sine-Gordon equation, Physica D 135 (2000) 345–368.
[7] T. Povich, J. Xin, A numerical study of the light bullets interaction in the $(2+1)$ sine-Gordon equation, J. Nonlinear Sci. 15 (2005) 11–25.
[8] A. Newell, J. Moloney, Nonlinear Optics, Addison-Wesley, Redwood City, CA, 1991.
[9] R. McLeod, K. Wagner, S. Blair, $(3+1)$-dimensional optical soliton dragging logic, Phys. Rev. A 52 (1995) 3254–3278.
[10] L. Bergé, T. Colin, A singular perturbation problem for an envelope equation in plasma physics, Physica D 84 (1995) 437–459.
[11] T. Brabec, F. Krausz, Nonlinear optical pulse propagation in the single-cycle regime, Phys. Rev. Lett. 78 (1997) 3282–3286.
[12] A.E. Kaplan, P. Shkolnikov, Electromagnetic "bubbles" and shock waves: unipolar, nonoscillating EM solitons, Phys. Rev. Lett. 75 (1995) 2316–2319.
[13] A.E. Kaplan, P. Shkolnikov, Subfemtosecond high-intensity unipolar electromagnetic soliton and shock waves, J. Nonlinear Opt. Phys. Mater. 4 (1995) 831–841.
[14] M. Agrotis, N.M. Ercolani, S.A. Glasgow, J.V. Moloney, Complete integrability of the reduced Maxwell–Bloch equations with permanent dipole, Physica D 138 (1–2) (2000) 134–162.
[15] R.M. Joseph, S.C. Hagness, A. Taflove, Direct time integration of Maxwell's equations in linear dispersive media with absorption for scattering and propagation of femtosecond electromagnetic pulses, Opt. Lett. 16 (1991) 1412.
[16] P. Kirrmann, G. Schneider, A. Mielke, The validity of modulation equations for the extended system with cubic nonlinearities, Proc. Roy. Soc. Edinburgh Sect. A 122 (1992) 85–91.
[17] R.D. Pierce, C.E. Wayne, On the validity of mean-field amplitude equations for counter-propagating wavetrains, Nonlinearity 8 (1995) 769–779.
[18] N. Akhmediev, A. Ankiewicz, Does the nonlinear Schrödinger equation correctly describe beam propagation? Opt. Lett. 18 (1993) 411–413.
[19] C. Sulem, P.-L. Sulem, The Nonlinear Schrödinger Equation, Self-Focusing and Wave Collapse, Springer-Verlag, New York, 1999.
[20] G. Fibich, G. Papanicolaou, Self-focusing in the perturbed and unperturbed nonlinear Schrödinger equation in critical dimension, SIAM J. Appl. Math. 60 (2000) 183–240.
[21] G. Fibich, G. Papanicolaou, A modulation method for self-focusing in the perturbed critical nonlinear Schrödinger equation, Phys. Lett. A 239 (1998) 167–173.
[22] Y. Siberberg, Collapse of optical pulses, Opt. Lett. 15 (1990) 1282–1284.
[23] J. Bourgain, Global Solutions of Nonlinear Schrödinger Equations, in: American Mathematical Society Colloquium Publications, vol. 46, American Methematical Society, Providence, RI, 1999.
[24] T. Cazenave, Semilinear Schrödinger Equations, in: Courant Lecture Notes in Mathematics, vol. 10, New York University Courant Institute of Mathematical Sciences, New York, 2003.
[25] P. Donnat, J. Rauch, Global solvability of the Maxwell–Bloch equations from nonlinear optics, Arch. Ration. Mech. Anal. 136 (1996) 291–303.
[26] A. Minzoni, N. Smyth, A. Worthy, Pulse evolution for a two dimensional sine-Gordon equation, Physica D 159 (2001) 101–123.
[27] A. Minzoni, N. Smyth, A. Worthy, Evolution of two-dimensional standing and traveling breather solutions for the sine-Gordon equation, Physica D 189 (2004) 167–187.
[28] M.J. Ablowitz, M.B. Herbst, C.M. Schober, On the numerical solution of the sine-Gordon equation: I. Integrable discretizations and homoclinic manifolds, J. Comput. Phys. 126 (1996) 299–314.
[29] M.J. Ablowitz, M.B. Herbst, C.M. Schober, On the numerical solution of the sine-Gordon equation: II. Performance and numerical schemes, J. Comput. Phys. 131 (1997) 354–367.
[30] B. Guo, P.J. Pascual, M.J. Rodriguez, L. Vázquez, Numerical solution of the sine-Gordon equation, Appl. Math. Comput. 18 (1986) 1–14.
[31] W.A. Strauss, L. Vázquez, Numerical solution of a nonlinear Klein–Gordon equation, J. Comput. Phys. 28 (1978) 271–278.
[32] M. Delfour, M. Fortin, G. Payne, Finite difference solution of a nonlinear Schrödinger equation, J. Comput. Phys. 44 (1981) 277–288.
[33] J.M. Sanz-Serna, Methods for the numerical solution of the nonlinear Schrödinger equation, Math. Comp. 43 (1984) 21–27.
[34] W. Bao, D. Jaksch, An explicit unconditionally stable numerical method for solving damped nonlinear Schrödinger equations with a focusing nonlinearity, SIAM J. Numer. Anal. 41 (2003) 1406–1426.
[35] W. Bao, S. Jin, P.A. Markowich, On time-splitting spectral approximations for the Schrödinger equation in the semiclassical regime, J. Comput. Phys. 175 (2002) 487–524.
[36] J. Shen, T. Tang, Spectral and High-Order Methods with Applications, Science Press, 2006.
[37] L.N. Trefethen, Spectral Methods in Matlab, SIAM (Socity of Industrial and Applied Mathematics), 2000.